Ocean Engineering 363 (2026) 126463

Contents lists available at ScienceDirect

Ocean Engineering

journal homepage: www.elsevier.com/locate/oceaneng

Research paper

Hydrodynamics of spar mounted OTEC system: An experimental and numerical study

N.V. Nasma Noor [a,c,*], V.K. Srineash [a], Manasa Ranjan Behera [a,b]

[a] Department of Civil Engineering, Indian Institute of Bombay, Mumbai, Maharashtra, India
[b] Centre for Climate Studies, Indian Institute of Bombay, Mumbai, Maharashtra, India
[c] Department of Civil Engineering, Govt Engineering College Kozhikode, Kerala, India

ARTICLE INFO

Keywords:
Hydrodynamics
Floating platform
Cold water pipe (CWP)
Experimental
Numerical
Ocean thermal energy conversion (OTEC)

ABSTRACT

Ocean Thermal Energy Conversion (OTEC) represents the second most promising energy potential among marine renewable sources. Mounting OTEC system on floating platforms could efficiently generate baseload power and freshwater for small island developing states reducing the fossil fuel consumption. A critical component of such systems is the Cold Water Pipe (CWP), whose integration with floating platforms introduces complex hydrodynamic and structural interactions. This study focuses on understanding the response behaviour of a spar-type floating OTEC platform with an attached CWP, combining both experimental and numerical investigations. Regular wave tests are performed for the spar with soft mooring, and the results are validated numerically. For numerical investigation the spar hull is modelled using a boundary element panel method for diffraction analysis, while the CWP is idealized as a rigid body connected to the spar. Time-domain simulations are conducted for operational regular wave conditions with and without the CWP to assess its effect on surge, heave, and pitch responses. The results demonstrate that the presence of the CWP significantly reduces pitch motion due to added damping and inertia effects, has minimum impact on heave, and can either amplify or reduce surge depending on the wave period. These findings emphasize the importance of including the CWP in coupled hydrodynamic analysis to capture realistic platform behaviour. The integration of a CWP with the spar significantly improves hydrodynamic performance, with reductions in mean amplitudes of up to 86% in surge, 37% in heave, and 97% in pitch. These improvements suppress coupling effects and mitigate parametric resonance, thereby enhancing stability and informing preliminary mooring design under diverse sea states. Overall, the study provides a comprehensive preliminary understanding of the hydrodynamic behaviour of spar OTEC platforms and offers guidance for future experimental and numerical investigations.

1. Introduction

Efforts to harness viable renewable energy from all possible sources are at their peak in both the industrial sector and academic and research institutions. The highly dynamic ocean offers several opportunities for energy extraction, including coastal-based systems and deep-ocean-based systems. Ocean Thermal Energy Conversion (OTEC) is one such deep-water energy generation technology capable of producing energy with net-zero carbon emissions, utilizing the temperature gradient between warm surface water and colder deep water. OTEC systems can be coastal, shelf-based, or offshore; however, commercially viable implementations are typically deep-water floating systems. The major components of a floating OTEC system, from a hydrodynamic perspective, are the floating platform, the Cold Water Pipe (CWP), and the mooring. The floating platforms commonly used for OTEC systems include spars, semi-submersibles, and barges or ships (Nasma Noor et al., 2024). The CWP draws deep cold water and feeds it into the condensation stage of the heat exchange system. The mooring system, which provides station-keeping, can be either taut or slack. Despite its promise on high potential, OTEC faces challenges related to both commercial viability and technical performance.

The dynamics of the deep water floating OTEC supporting structure are examined in this study by employing both experimental and numerical approaches. Spar platforms exhibit significantly lower surge, heave, and pitch responses compared to semi-submersibles under similar wave and cost conditions, making them more stable and suitable

* Corresponding author. Department of Civil Engineering, Indian Institute of Bombay, Mumbai, Maharashtra, India.
E-mail address: nasmanoornv@gmail.com (N.V. Nasma Noor).

https://doi.org/10.1016/j.oceaneng.2026.126463
Received 30 October 2025; Received in revised form 17 May 2026; Accepted 6 June 2026
Available online 17 June 2026

for deepwater applications (Kaptan et al., 2022; Nallayarasu & Kumar, 2017). Spar platforms are also favoured for their ability to support dry tree production and rigid risers in deepwater, owing to their reduced sensitivity to environmental loads and relatively simpler mooring requirements (Ma and Patel, 2001). Recent reviews on multi use offshore platforms emphasize the growing trend of combining renewable energy systems such as wind, wave, solar, and OTEC with aquaculture facilities. Within such designs, spar type floating structures are consistently identified as the most suitable option for deepwater deployment, where fixed foundations are impractical and stability requirements are more demanding (Manolache and Andrei, 2024). The COSPAR prototype study (Chu and Wang, 2020) demonstrated that spar platforms integrated with aquaculture cages exhibit superior hydrodynamic performance, minimizing heave and pitch motions more effectively than other floating configurations. Consequently, spar configurations are increasingly regarded as a future ready solution for large scale deep sea applications, offering both motion stability and design flexibility for multiuse operations.

Both spar-type Floating Offshore Wind Turbines (FOWTs) and spar-type OTEC platforms utilize deep-draft cylindrical structures, but their hydrodynamic behaviours differ markedly due to design intent and geometry. The spar FOWT employs a much smaller diameter, reducing wave excitation and viscous drag while maintaining high stability in deep waters (Zeng et al., 2024). Its responses are primarily influenced by wave-current interactions and nonlinear mooring dynamics, which significantly affect tower base fatigue and cable tension(L. Chen and Basu, 2018). Conversely, the spar OTEC platform features a larger diameter to house heavy thermal equipment and the CWP resulting in increased added mass and damping (Nasma Noor et al., 2024). The CWP platform coupling and moonpool dynamics dominate its hydrodynamic response, making it distinct from FOWTs in terms of motion behaviour and structural design. Herrera et al. (2021) noted that as OTEC systems are deployed further offshore and into deeper waters, they encounter greater challenges from stronger currents, wave loads, and increased stresses along the extended CWPs. The review emphasizes that platform stability is crucial in mitigating these stresses, with spar structures offering distinct advantages due to their deep draft geometry that inherently minimizes heave and pitch motions. This makes spar configurations attractive for future deepwater OTEC applications where the reliability and structural integrity of the cold water intake system are of paramount importance.

Despite the well-known advantages of spar platforms, parametric excitation and heave-pitch coupling represent important nonlinear dynamic behaviours in slender floating offshore structures (Yang and Xu, 2015). Experimental and numerical investigations have demonstrated that coupled heave-pitch resonance can significantly influence motion responses, stability (Davidson et al., 2022), and overall platform performance, with Mathieu-type instabilities observed under both regular and irregular wave conditions (Nallayarasu & Senthil Kumar, 2017). Several analytical and numerical approaches have been proposed to predict and mitigate parametric resonance by appropriately modifying system parameters such as waterplane area and metacentric height (Yang and Xu, 2015; Yue et al., 2020). The effectiveness of modern numerical tools for analysing parametric and combination resonance through time-domain simulations has been demonstrated in previous studies (Choi et al., 2016; Nallayarasu & Kumar, 2017).

The CWP differs fundamentally from risers in oil and gas platforms, as it is specifically designed for seawater intake, whereas risers are slender conduits primarily serve the purpose of fluid transport (Nasma Noor et al., 2024). According to API recommended guidelines, riser diameters typically range from 0.15 to 1.2 m. In the literature, the ratio of CWP diameter to riser diameter has been reported to vary between 4 and 10. Fig. 1 presents the diameters of risers and CWP summarised from the literature (Maris and Paulling, 1980; Nihous and Vega, 1993; Pesce and Martins, 2005; Salama et al., 2002; Tarnopol'skii et al., 1999; Ward et al., 2007; Wu, 2020; Yang et al., 2012; Yin et al., 2019). Compared to risers, CWP is unique due to its large diameter, high diameter to thickness ratio, material properties, connection details, and the number of joints along the pipe (Nasma Noor et al., 2024). Exclusive studies on past pilot projects attempting OTEC energy production have indicated a relationship between the targeted power output and the diameter of the CWP. In addition, Yeh et al. (2005) theoretically established the dependence of net power on pipe diameter for efficient power generation. These findings highlight the need for larger diameter pipes. Fig. 2

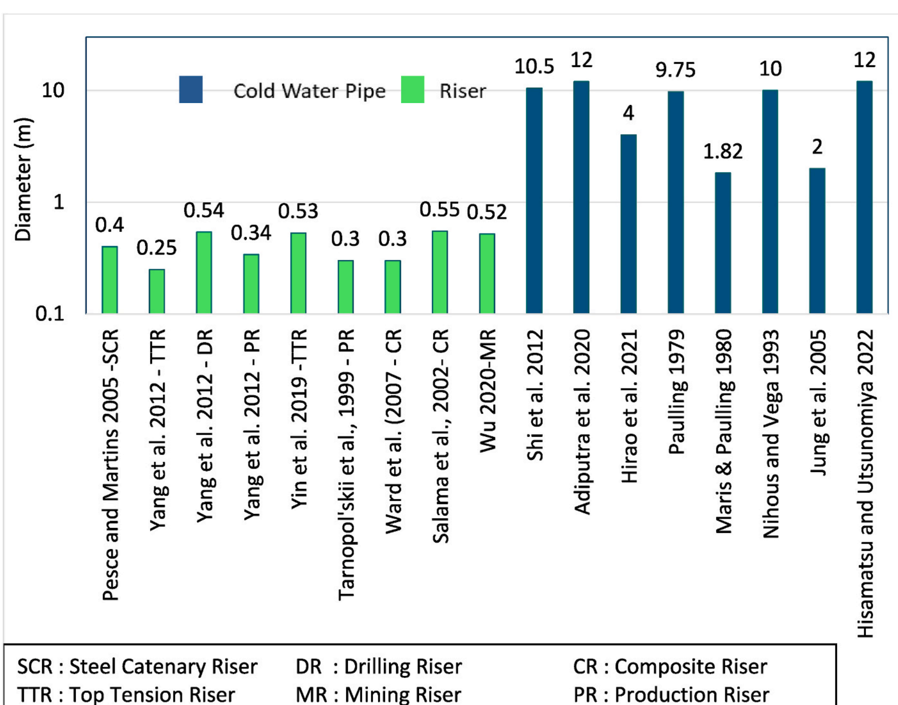

Fig. 1. Typical Riser diameter and CWP diameters in literature.

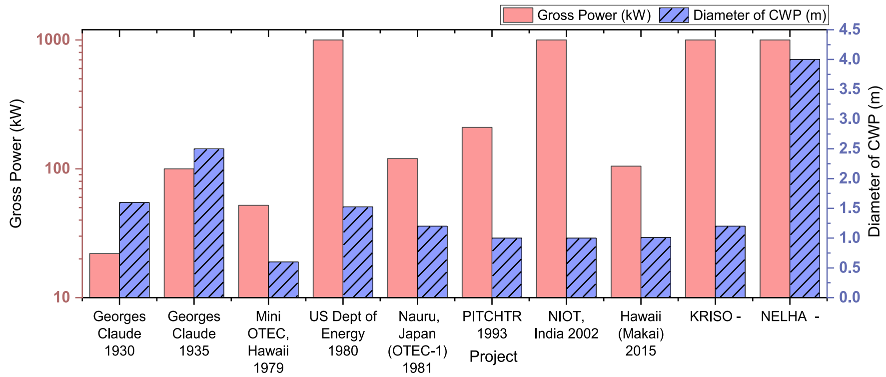

Fig. 2. Relationship between gross power and diameter of CWP from past OTEC projects.

presents the dependence of diameter of the CWP on the gross power of the platform. The dynamic behaviour of the platform is coupled to the CWP and mooring (Hisamatsu and Utsunomiya, 2022). The presence of a CWP can introduce additional hydrodynamic loads and motions to the floating platform (Adiputra et al., 2024). Due to its large size and flexibility, accurately modelling the hydrodynamic behaviour of a CWP poses significant challenges. There are limited experimental studies on floating platforms with integrated CWPs, and available experimental facilities often face constraints in replicating realistic conditions at scale. As a result, the validation of numerical results for platform CWP interactions remains a major barrier in advancing reliable design and analysis methods.

A concise historical overview of OTEC research is available in the literature (Aresti et al., 2023; Nasma Noor et al., 2024). Subsequent studies in the 2000s explored alternative CWP materials and the development of composite pipes (Miller and Ascari, 2011; Shi et al., 2012). Jung et al. (2005) introduced a finite difference model for free-hanging pipes under vibration in calm water. More recently, advanced tools such as WAMIT, Flexcom, RIFLEX, and Orca Flex were used to model the coupled hydrodynamic responses of CWPs with various floating platforms, including semisubmersibles, spars, and moored ships (Hirao et al., 2021; Hisamatsu and Utsunomiya, 2022; Shi et al., 2012). Similarly, Spanos et al. (2010) developed a coupled model for spar risers, while Adiputra et al. (2019) focused on numerical optimization for OTEC plant incorporating large FRP pipes. Research on CWP also referred as sea water intake risers (SWIR), is advancing at a commendable pace, with particular emphasis on understanding VIV, addressing nonlinear dynamic behaviour, and optimization of clump weights and pipe geometry. Y. Ma et al. (2023) has provided a detailed summary of experimental studies on the water conveying fluid pipes. Scaled physical model studies have yielded valuable insights into the stability and performance of CWPs under harsh environmental conditions (Guo et al., 2024; Y. Ma et al., 2023). Collectively, these studies demonstrate significant progress in understanding the dynamics of CWPs through both experimental and numerical investigations.

The dependence of CWP dynamics on platform motions has been clearly highlighted in several recent studies (Adiputra et al., 2024; Cai et al., 2025). Most of these investigations have focused on ship or vessel shaped floating structures for economic reasons. Table 1 summarises the literature on floating OTEC platform hydrodynamics, covering aspects such as type of structure, mooring arrangement, research methodology, metocean conditions, and whether the CWP was considered in the analysis. Only a limited number of studies have examined spar and semisubmersible platforms, and even among these, the motion response associated with CWP is yet to be comprehensively understood. For instance, Hirao et al. (2021) quantified the coupled response of the platform and CWP through both experimental and numerical approaches, under conditions with and without internal flow. However, their analysis was restricted to a configuration with horizontal mooring, which is not commonly adopted in practical OTEC systems. Although several researchers have studied on various platform configurations for OTEC and desalination applications (Guo et al., 2024; Vishwanath and Jalihal, 2022), many of these did not incorporated CWP in their analysis (D. Y. Lee et al., 2015; Vishwanath and Jalihal, 2021). The continued scarcity of reliable experimental data remains a key limitation in developing robust numerical models capable of accurately representing the coupled behaviour of the platform and CWP.

To begin with, the floating spar platform without the CWP is modelled with a horizontal mooring system and tested in regular waves. The numerical model of the identical system is then developed, incorporating the damping values obtained from the experiments to ensure realistic motion representation. The results obtained from the numerical simulations are validated using the experimental data. Subsequently, numerical simulations were performed for a spar with a CWP, and the results were compared with published data for verification (Nasma et al., 2025). After establishing sufficient confidence in the adopted numerical methodology, time domain response analysis is carried out for the selected wave environment to examine the influence of the CWP on the response of taut moored spar platform. The analysis is performed for both configurations, spar with and without a CWP, under wave as well as combined wave and current conditions.

2. Methodology

To understand the platform response of an OTEC system, a hybrid methodology is adopted that combines experimental and numerical methods. Floating platforms can be modelled relatively easily for physical experiments. However, modelling the mooring system and CWP demands large testing facility in terms of both size and depth. Even with such a facility, achieving geometric and dynamic similitude for the CWP and mooring remains highly challenging. The proposed methodology can therefore be adopted for the preliminary understanding of the platform response with the CWP and mooring. The following Fig. 3 illustrates the adopted methodology. A potential flow based solver is used for the numerical modelling of floating platform with CWP.

Numerical investigation using tools like AQWA, when supported by flume test results, helps overcome the limitations of experimental wave-structure studies such as restricted basin size, wave reflections, and scaling issues (Hegde and Nallayarasu, 2023). This combined approach enables a preliminary investigation of hydrodynamic behaviour, accounting for mooring effects and platform responses across a range of wave conditions, including extreme cases that are often difficult to reproduce accurately with physical models alone.

A spar platform for an OTEC system was selected, and its geometric modelling was carried out considering the constraints of the available experimental facility. The model was fabricated and tested at a scaled

Table 1
Literature on hydrodynamics of floating OTEC platforms.

Literature	Floating structure			CWP	Mooring			Method			Wave Environment			Current
	Spar	Semi-Submersible	Ship/Vessel		Horizontal	Taut	Slack	Experimental	Numerical	Analytical/Semi Analytical	Regular	Random	Extreme	
Barr and Sheldon (1980)			✓	✓				✓				✓		
Hong et al. (2004)			✓	✓			✓	✓				✓	✓	
Shi et al. (2012)		✓		✓		✓			✓			✓		✓
Xiang et al. (2013)			✓	✓					✓			✓	✓	✓
Halkyard et al. (2014)		✓		✓	✓			✓	✓		✓	✓	✓	
Lee et al. (2015)	✓										✓	✓		✓
Wang et al. (2016)			✓	✓				✓						
Hirao et al. (2021)	✓			✓	✓			✓	✓		✓	✓		✓
Vishwanath and Jalihal (2021)	✓						✓		✓			✓	✓	✓
Vishwanath and Jalihal (2022)	✓	✓					✓		✓			✓		
Hisamatsu and Utsunomiya (2022)			✓	✓		✓			✓	✓			✓	✓
Zhang et al. (2023)				✓					✓	✓				
Guo et al. (2024)	✓	✓		✓	✓				✓			✓	✓	✓
Faizatama et al. (2025)			✓	✓			✓	✓	✓			✓		✓
Present Study	✓			✓	✓	✓		✓	✓		✓	✓	✓	✓

downsize and it was redesigned as necessary until the key parameters were within acceptable tolerance limits. Determining the damping parameters was essential for the numerical analysis, these values were used as user defined inputs in the numerical model. All relevant data from the physical model tests were incorporated into the numerical setup, and the experimental and numerical results were validated for both the free decay tests and wave structure interaction studies. The next step involved the validation of the spar with the attached CWP through numerical simulations, using published results as a reference. With these validations complete, the model became ready for simulations under various wave conditions. This approach helps in quantifying the percentage deviation in the platform response when comparing the spar alone with the spar fitted with the CWP. Fig. 4 shows the schematic diagram of the various analysis stages. Details of the experimental and numerical investigations are presented in the subsequent sections.

2.1. *Experimental investigation*

2.1.1. *Model description*

A classical spar model was selected for experimental analysis. A simple cylindrical hull with a moonpool was used in the study (Hirao et al., 2021). A model scale of 1:175 was adopted considering the wave flume limitations and Froude modelling principles. The geometric modelling of the scaled model was carried out in SOLIDWORKS. The scaled down values of weight, centre of gravity, and moment of inertia were maintained equivalent to those of the full scale model. Several trials were conducted to achieve appropriate values with accuracy within specified tolerance levels (Chakrabarti, 1994). The model consists of a 3D printed hull and steel ballast weights. The Hull section was printed in two stages using the 3D printing facility in the Ocean Engineering lab of IIT Bombay. The printing material used was PLA (Polylactic Acid) with a density of 1200 kg/m^3. The geometric details and static parameters of the spar model are shown in Table 2.

Various stages in the fabrication and assembly of the model along with final assembled unit are shown Fig. 5 below. The final assembled model was painted and tested for any leakage in the wave flume. The weight of the model was measured before and after being submerging it in water for 24 h, with the difference calculated after thoroughly drying the model. In case of any detected leakage was detected, necessary repairs were carried out.

2.1.2. *Preliminary tests*

The fabricated model was examined for accuracy against the designed values, including centre of gravity, draft, and moment of inertia. As part of this process, the centre of gravity was determined through a suspension test, in which the model was suspended on a knife edge and weights on either side were balanced. The measured location of this point was then compared with the designed values. Once the centre of gravity was established, a bifilar suspension test was conducted to determine the moment of inertia (Xu and Day, 2021). This test involved suspending the model using two threads placed at equal distances on either side of the centre of gravity. A small disturbance was applied to the model to initiate the oscillation, and the corresponding natural period was recorded. Since the spar model is symmetric about the z axis, the roll and pitch moments of inertia were considered equal. The mass moment of inertia was then calculated using the following formula:

$$I = \frac{mgD^2T^2}{(4\pi)^2 h^2} \quad \text{Eqn 1}$$

Where, T is the natural period of the oscillation, m is the mass of the model, D is the distance between the threads and h is the height of the suspended thread. For precise measurements, the times for three and six oscillations were recorded to calculate the natural period in six independent trials. In the present test, D was 12 cm, and h was 61.4 cm, and

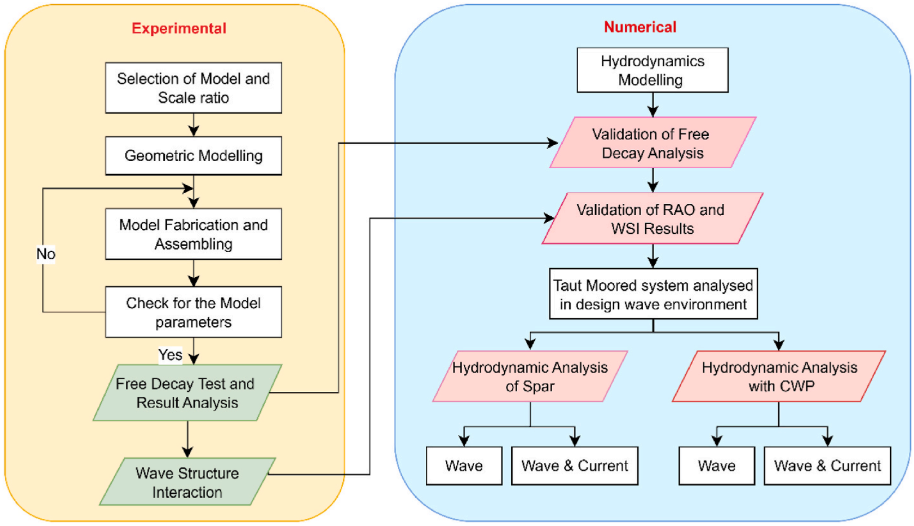

Fig. 3. Methodology adopted for the study.

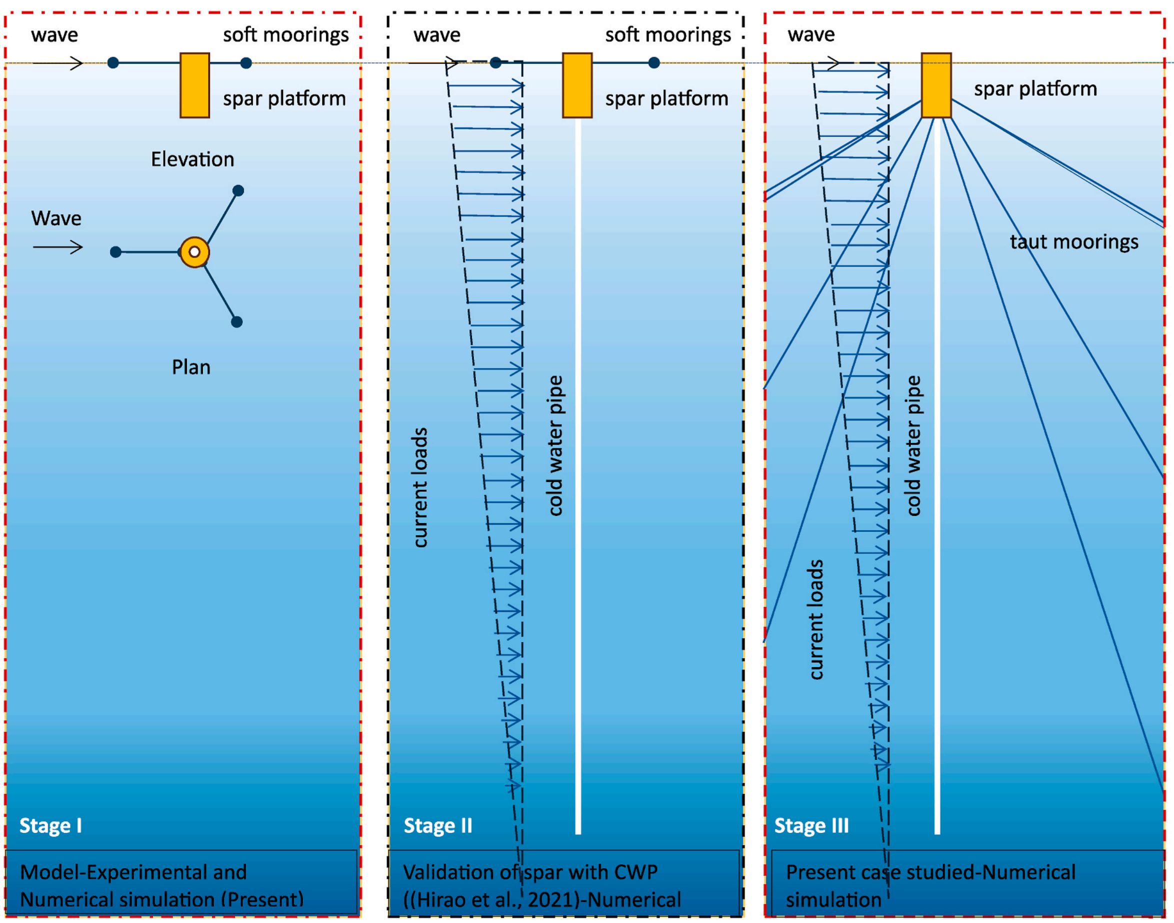

Fig. 4. Schematic diagram of the different stages of analysis (i) experimental and numerical model of the spar (ii) horizontal moored spar floating platform with CWP for validation (iii) taut moored spar with CWP -present simulation.

the observed natural period was 4.89 s. Fig. 6 illustrates the test setup for suspension test and bifilar test.

The obtained results were checked for tolerance levels following the procedure for experimental modelling (Chakrabarti, 1994). The designed and fabricated values are presented in a manner similar to those reported by Wang et al. (2016) and are listed in Table 3. Hydrostatic tests were performed to verify the stability and draft of the model. The discrepancies between the designed and experimentally measured values (Zhai et al., 2025) of the model were carefully calculated. The results indicated that these deviations fall within acceptable limits (Chakrabarti, 1994), confirming the reliability and accuracy of the experimental measurements.

Table 2
Geometric and hydrostatic parameters of the model.

Parameter	Model
Diameter hull (m)	0.2
Diameter of moonpool (m)	0.034
Height (m)	0.477
Draft (m)	0.4
Displacement (m^3)	0.012202915
Area (m^2)	0.030492683
CG from Bottom (m), KG	0.114
GM (m)	0.0921
Kxx = Kyy (m)	0.188
Kzz (m)	0.705

2.1.3. *Test facility and instrumentation*

The fabricated model was tested in the wave flume of Ocean Engineering Laboratory at IIT Bombay, India. The flume is 40 m long, 1 m wide and 1.25 m deep with an additional pit 1 m deep and 1.3 m wide located at its centre. One end of the flume is equipped with a piston type wave maker for wave generation, while the opposite end incorporates an artificial absorbing beach to minimize wave reflection. The wave maker comprises precisely engineered mechanical components driven by servo motors and governed by an advanced control mechanism, facilitating the generation of waves with predefined amplitude and frequency. The system is capable of producing two dimensional regular and random waves, as well as user defined wave series, including extreme or freak waves (Rambabu and Srineash, 2025; Sashank et al., 2026). The wave absorbing beach comprises a rubble mound overlaid with a sloping porous plate, which effectively dissipates wave energy and reduces reflection back into the flume. In addition, the flume is equipped with a current generation system, enabling experiments under combined wave-current conditions. A 3 m long glass walled section is installed in the centre of the wave flume, providing visual access from the sides, allowing a better understanding of wave structure interaction phenomena.

The motion of the model was captured using six degrees of freedom (6-DOF) Inertial Measurement Unit (IMU) sensor MT- G710 by XSens. During the experiments, the moonpool was configured as open to the atmosphere (Bull, 2015), following the conventional experimental arrangement adopted in earlier studies (Liu et al., 2014; Pham and Shin, 2019; Shahabadi et al., 2017). The IMU sensor was positioned at the centre of the moonpool, with adequate clearance from both side walls to ensure accurate measurements. The sensor records accelerations in three

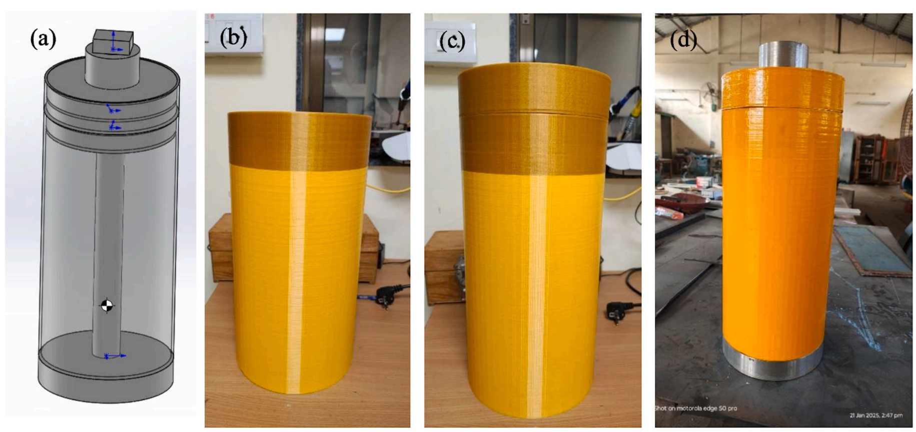

Fig. 5. (a) Modelled Geometry in SOLIDWORKS (b) 3 d printed bottom hull (c) bottom hull and top hull (d) Assembled model.

Fig. 6. (a) Suspension test and (b) bifilar test on the assembled model.

Table 3
Physical properties of the model.

Parameter (m)	Full scale	Model scale (designed)	Model scale (Measured)	Percentage Error (%)
Outer Diameter	35	0.200	0.201	0.5
Moon pool diameter	6	0.034	0.034	0.5
Height	83.5	0.477	0.478	0.2
Centre of gravity	20	0.114	0.117	2.6
Draft	70	0.400	0.414	3.5
Radius of gyration -pitch	33	0.188	0.182	2.7

translational degrees of freedom, and rotations in roll, pitch, and yaw, at a maximum sampling frequency of 400 Hz. For the present experiment, a sampling frequency of 100 Hz was selected. The measured accelerations were converted into corresponding displacements using Fast Fourier Transform (FFT) algorithm. The water surface elevations were measured using two wave probes, one placed 8 m (Aiswaria et al., 2024; Sashank et al., 2026) from the paddle (P1) and another positioned (P2) one wavelength seaward of the model. The wave probes were calibrated prior to the experiment, and calibration ratio was determined. The data acquisition (DAQ) system records the raw voltage output from the wave probe, which is subsequently converted into wave height through the application of a calibration constant. This calibration procedure ensures that the probe's electrical response is accurately translated into the corresponding physical wave elevation, thereby enabling the DAQ to provide reliable wave height measurements. The wave elevations from both probes were recorded at a sampling frequency of 100 Hz.

2.1.4. Station keeping of the model

Floating bodies were held in position by mooring lines. The mooring arrangement in real sea state could generally be of either the taut or catenary type. Experimental modelling of catenary or taut mooring was often challenging in most of the situations due to the width and depth constraints of the testing facilities. The International Towing Tank Conference (ITTC, 2017) recommended the use of soft mooring in wave flumes with space constraints. Soft mooring can adequately model the restraint conditions (Rony et al., 2026; Thomas et al., 2024). The stiffness of the restraining system should be modelled such that natural period of the restraining system should be one order greater than the lowest wave period and the natural period of the model.

The effective stiffness of the model was determined for the proposed mooring configuration, and the stiffness of the individual springs was calculated to comply with the ITTC Recommended Procedures and Guidelines for Floating Offshore Platform Experiments (ITTC, 2017). The mooring arrangement are shown in Fig. 7. The natural period, T_s of the restraining system is expressed by the *Eqn* 2 (Lee et al., 2023), where

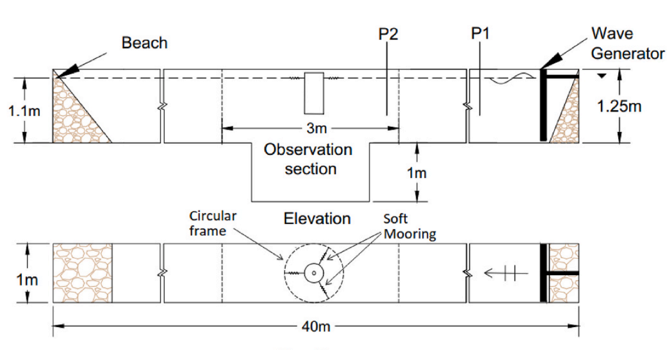

Fig. 7. Schematic diagram of arrangement of model in the wave flume.

M is the mass of the model, M_a is the added mass of the model and K_{eff} is the equivalent stiffness. Three springs of equal stiffness were connected at 120° intervals around the model. The lowest wave period of the test was 0.91 s, and the stiffness of restraining system was calculated using *Eqn* 2. For the selected spring arrangement, the law of motion was applied, and the stiffness of the individual springs (K) was obtained using *Eqn* 3. The required stiffness of the individual spring should be less than 6.5 N/m.

$$T_s = 2\pi\sqrt{\frac{M + M_a}{K_{eff}}} \quad \text{Eqn 2}$$

$$K_{eff} = \frac{2}{3}K \quad \text{Eqn 3}$$

The model was placed at the mid length of the test section, and three springs were used to position the model during the wave structure interaction tests. Springs of stiffness 5.2 N/m and unstretched length of 90 mm, made of AISI 316 stainless steel, were used. The fairlead points were fixed at the waterline of the model, and the anchor points were attached to a circular frame with radius of 0.5 m. The schematic diagram of the setup is presented in Fig. 7.

2.1.5. Free decay tests

The natural periods of the model in heave and pitch were determined by conducting free decay tests. The model was released from all supports and subjected to an initial displacement in the heave direction and an initial angular disturbance in the pitch direction. The 6-DOF motion sensor attached to the model recorded the resulting accelerations and rotations. Multiple trials were performed to confirm the repeatability of the observed behaviour. The recorded accelerations were converted to displacements using the FFT algorithm (Nallayarasu & Senthil Kumar, 2017). The natural frequency and damping ratio of the model were then determined using the logarithmic decrement method.

The logarithmic decrement δ was calculated from the decay curve using:

$$\delta = \frac{1}{n} ln\left(\frac{x_0}{x_n}\right) \quad \text{Eqn 4}$$

where x_0 is the initial peak amplitude x_n and is the peak amplitude after n cycles. The damping ratio ζ was then obtained from:

$$\zeta = \frac{\delta}{\sqrt{4\pi^2 + \delta^2}} \quad \text{Eqn 5}$$

The natural frequency of the model in heave and pitch was calculated using the following formula, where ω_d is the damped natural frequency:

$$\omega_n = \frac{\omega_d}{\sqrt{1 - \zeta^2}}; \quad where \quad \omega_d = \frac{2\,\pi\, n}{(t_n - t_0)} \quad \text{Eqn 6}$$

The equivalent viscous damping coefficient in heave and pitch was calculated using:

$$C = 2\,\zeta\,\omega_n\sqrt{K(M + M_a)} \quad \text{Eqn 7}$$

where M is the mass (for heave) or mass moment of inertia (for pitch), M_a is the added mass (heave) or added mass moment of inertia (pitch), and K is the hydrostatic restoring stiffness. The restoring stiffness in heave (K_{33}) and pitch (K_{55})values were computed using:

$$K_{33} = \rho g A_{wp};\; K_{55} = Mg\, GM_L \quad \text{Eqn 8}$$

Where ρ is the water density, g is gravity, A_{wp} is the waterplane area and GM_L is the metacentric height.

The viscous damping component derived from these tests was used as input for the numerical simulations, while the natural frequency was used to determine the appropriate wave period range for the experiments.

2.1.6. Regular wave tests

Wave response studies in regular waves were conducted for a total of six wave heights and eight wave periods. The selection of wave periods was based on the design wave height relevant to Indian metocean conditions (Haripriya et al., 2021; Sreelakshmi and Bhaskaran, 2020), ensuring that all tests satisfied deep water criteria. A minimum interval of 15 min was maintained between successive trials to allow the water and model to settle. Prior to testing, the wave probes were calibrated. The water depth was maintained at 110 cm throughout the experiments. The experimental program considered a range of relative water depth ratios (d/L) varying from 0.5 to 0.85 in increments of 0.05, where d is the water depth and L is the wavelength. Corresponding wave periods (T) were calculated for each d/L value. Six wave heights were selected at the model scale, based on the design wave height reported in the literature (Vishwanath and Jalihal, 2021), considering a range on either side of this value, with wave steepness ranging from 0.01 to 0.04. These correspond to prototype wave heights of approximately 4 m to 9 m. The selected heights represent a range of realistic design wave conditions for Indian waters while ensuring compliance with the deep water wave criteria in the experimental setup. Table 4 presents the test matrix considered for the regular wave tests.

In each test, wave elevations and model responses were recorded at a sampling frequency of 100 Hz for a duration of 60 s. For every change in wave period, the second wave probe located near the model was repositioned to a distance one wavelength seaward of the model. The primary responses of a spar type platform occur in surge, heave, and pitch. Since the surge response is strongly influenced by the type of mooring system, the present study focuses on the heave and pitch responses. The hydrodynamic behaviour of the spar model in heave and pitch was characterized using Response Amplitude Operators (RAOs), derived from the experimental measurements. The RAOs were determined using the energy spectral method (O'Donnell et al., 2021). Here, RAO is defined as the square root of the ratio between the energy density spectra of the output response signal ($S_{xx}(\omega)$) and the input wave elevation signal ($S_{\eta\eta}(\omega)$), expressed as:

$$RAO = |H(\omega)| = \left[\frac{S_{xx}(\omega)}{S_{\eta\eta}(\omega)}\right]^{1/2} \quad \text{Eqn 9}$$

The energy density spectra, also known as the power spectral density, is obtained by applying the fast Fourier transform to the wave elevation or response time series. Fig. 8 shows the model supported by the horizontal springs and the image during testing.

2.2. Numerical investigation

In this section, the numerical model of the spar platform is developed using the linear potential flow theory in the ANSYS Hydrodynamic Diffraction module (AQWA) (ANSYS, 2022), which employs panel method to solve the boundary value problem (Faizatama et al., 2025). The geometric model is complemented with essential physical parameters such as centre of gravity, mass, and moments of inertia obtained from physical measurements and supplied as inputs to the numerical simulation. To ensure the numerical predictions closely replicate the physical behaviour observed in wave flume experiments, damping characteristics obtained from free decay tests were utilized. The total damping estimated from the experiments includes both radiation and viscous components. AQWA internally calculates radiation, while the difference between the total experimentally derived damping and simulated radiation damping is provided as an additional user defined viscous damping input. This adjustment ensures closer agreement with the observed motion responses. The spar is modelled as a diffracting body, with its wetted surface discretized into diffracting elements for hydrodynamic analysis and CWP in Morison regime. Both the bodies were treated as two hydrodynamically interacting components rigidly connected together, there by responding as a single coupled system with six degrees of freedom. The free surface and body boundary conditions were modelled according to the linear potential flow assumptions (Faizatama et al., 2025). The moonpool was modelled as an open internal water region connected to the external fluid domain through the bottom opening, and its hydrodynamic behaviour was represented through the diffraction radiation panel solution on the wetted surfaces (Chuang et al., 2021; H. Liu et al., 2022). A time step corresponding to at 100 Hz was adopted to ensure numerical stability, and each simulation was run for a sufficient duration of 3600 s (Liu et al., 2025). The initial

Table 4
Test matrix for regular wave.

Case	d/L	Time Period (s)		Wave heights					
		Model	Full						
RW1	0.5	1.19	15.73	Model Scale (cm)					
RW2	0.55	1.13	14.99	2.29	2.86	3.43	4.00	4.57	5.14
RW3	0.6	1.08	14.34						
RW4	0.65	1.04	13.78						
RW5	0.7	1.00	13.27	Full Scale (m)					
RW6	0.75	0.97	12.82	4	5	6	7	8	9
RW7	0.8	0.94	12.41						
RW8	0.85	0.91	12.04						

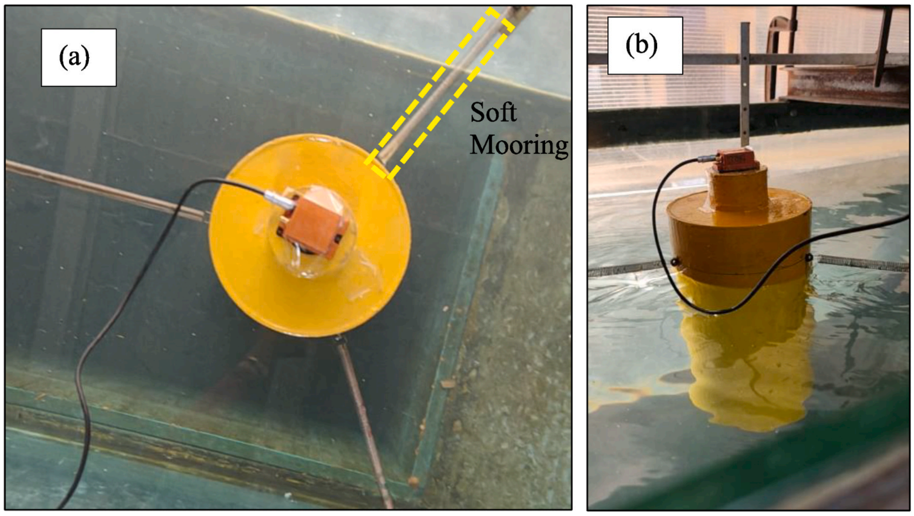

Fig. 8. (a) Model in the wave flume (b) model during testing.

conditions correspond to the still-water equilibrium position of the system. Once the setup was complete; the model was ready for numerical simulation.

Hydrodynamic parameters such as added mass, damping, restoring stiffness, and wave excitation forces are first obtained from frequency domain diffraction analysis. These are then utilized in time domain simulations based on Cummins' equation (Cummins, 1962) to predict the platform's motion response under specified wave conditions. The equation of motion used in the time domain simulation of the numerical model (Aqwa, 2022; Arya et al., 2026; Li and Choung, 2021) is expressed as:

$$[M+A_{\infty}]\ddot{X}(t)+C\dot{X}(t)+KX(t)+\int_0^t R(t-\tau)\dot{X}(\tau)d\tau=F_w(t)+F_c(t)+F_t(t)+F_m(t) \quad \text{Eqn 10}$$

Where $X(t)$ is the six DOF motion vector of the coupled spar CWP system, containing translational and rotational responses. M is the structural mass and inertia matrix of the complete system, including the contributions of the platform and the attached CWP elements. A_{∞} is the added-mass matrix at infinite frequency, representing the inertia of the surrounding fluid accelerated with the structure. C is the system damping matrix, while K is the total stiffness matrix, comprising the linear hydrostatic restoring stiffness together with additional stiffness contributions, such as those arising from mooring lines or articulations. The convolution integral containing $R(t-\tau)$ represents the impulse response function, accounting for fluid forces generated by past motions of the body. On the right-hand side, $F_w(t)$ is the wave excitation force vector, consisting of the incident-wave Froude-Krylov and diffraction force components. $F_c(t)$ represents the current-induced environmental loads. $F_t(t)$ is the mooring-line tension force vector acting on the platform. $F_m(t)$ denotes the total hydrodynamic force contribution from the Morison-modelled CWP elements, including drag and inertia forces evaluated from the instantaneous relative fluid structure kinematics and assembled into the global equation of motion at each time step.

The model accounts for motion in all six degrees of freedom and enables a comprehensive evaluation of the platform's dynamic behaviour under wave loading. The effect of ocean current was incorporated through a prescribed depth varying velocity profile (Vishwanath and Jalihal, 2021), The current induced loads on the platform were evaluated by accounting for the combined wave current interaction effects, wherein the steady current modifies the wave kinematics and induces additional drag and inertia forces on the structure.

The number of elements influences the computational efficiency and accuracy of the numerical model. To determine an appropriate mesh size, the same set of analyses was performed using four different mesh configurations. The results from the mesh sensitivity analysis, particularly the heave free decay response, were compared with experimental data. Based on the correlation with the experimental results, a suitable mesh size was selected for further simulations. Stability and free decay analyses were performed to determine the natural period of the system followed by numerical simulations for the selected metocean conditions. In the present numerical model, the nonlinear hydrostatic and Froude-Krylov forces are evaluated at each time step over the wetted surface, based on the instantaneous incident wave elevation (Aqwa, 2022; Yue et al., 2020). This formulation results in time-varying restoring forces that may induce parametric (Mathieu-type) resonance. Although the simulations were conducted under irregular JONSWAP wave conditions, the model inherently captures the mechanism capable of exciting parametric responses (Nallayarasu & Senthil Kumar, 2017; G. Wang et al., 2024).

The primary objective of this simulation is to understand the effect of the long cold-water pipe (CWP) associated with the OTEC plant on the platform motions. The limited depth of the flume restricts the physical modelling of the CWP, and it is challenging to achieve an exact scale ratio due to material selection and the pipe's elastic properties. Therefore, the numerical simulation is intended to address this limitation and could give a preliminary understanding about the behaviour of the system. Subsequent sections provide a detailed description of the modelling of the CWP and the mooring system.

2.2.1. Modelling of cold water pipe

The cold water pipe (CWP) is a unique and critical component of any OTEC system, responsible for drawing cold water from deep ocean layers to condense the working fluid. Also known as vertical cantilever pipe, its size, diameter, length, and material are key design parameters for an OTEC plant. In the present study, the structural flexibility of the CWP is beyond the scope of the analysis; therefore, the pipe was modelled as a rigid body.

The CWP attached to the floating platform was modelled as a free flooded pipe (Guo et al., 2024) rigidly connected to the spar platform using a series of Morison elements to capture its hydrodynamic and structural behaviour under wave loading. The CWP, being rigid, long and slender, was discretized into multiple segments (Liang and Peng, 2023; Y. Ma et al., 2023) by defining nodes at regular intervals along its length, typically every 2 m. These nodes were connected by line elements characterized by their diameter, drag coefficient ($C_{d)}$, and inertia coefficient (C_m). Six degrees of motion were considered for each CWP segment in its local coordinate system consisting of three translational and three rotational degrees of freedom, with the local x-axis defined along the longitudinal direction of the pipe element while the remaining local axes were oriented normal to the pipe axis (Aqwa, 2022). The hydrodynamic force on each segment was calculated using the Morison equation. The expression for the fluid forces acting on the cross section of a slender structural member is given as:

$$dF = \frac{1}{2}\rho\, C_d D\left|u_f - u_s\right|\left(u_f - u_s\right) + \rho A C_m \dot{u_f} - \rho A C_a \dot{u_s} \qquad \text{Eqn 11}$$

Where ρ is the fluid density, A is the projected area, D is the characteristic diameter, u_f and $\dot{u_f}$ are the water particle velocity and acceleration, u_s and $\dot{u_s}$ are the segment's velocity and acceleration. The top end of the CWP was rigidly connected to the floating platform using the fixed-point to body connection type, allowing it to move consistently with platform motions in all six degrees of freedom. To realistically simulate tension behaviour and minimize oscillations, a clump weight was added at the bottom of the pipe by assigning extra mass to the lowest node. This represents the gravitational and inertial effects at the free end. Clump weights, modelled as concentrated point masses at the bottom, play a key role in damping the translational motion of the CWP (Adiputra and Utsunomiya, 2019). The element length was chosen to be as practicable, and the forces and moments on the element are obtained by integrating on the element. Three-point Gaussian integration is used to evaluate the hydrodynamic forces and moments on each element. The forces and moments acting on each tube element are converted to the fixed reference axes, and the moments are calculated about the structure's centre of gravity. The overall fluid load is obtained by summing the forces from all tube and panel elements. The Morison elements were used in conjunction with the radiation and diffraction forces obtained from the hydrodynamic diffraction radiation analysis. These forces were incorporated through Cummins' convolution based formulation, enabling time domain simulation of the coupled system. The interaction of wave loading on both the platform and the discretized pipe segments enabled the evaluation of the dynamic response of the entire floating system under realistic sea conditions.

The dimensions and other specifications of the pipe were adopted from Hirao et al. (2021), as listed in Table 5. The added mass (Ca) and drag coefficient (Cd) of CWP were taken as 1.0 (Zhang et al., 2023). Adiputra and Utsunomiya (2021) studied the effect of added mass on the critical velocity and demonstrated that a constant added mass coefficient of 1.0 is appropriate for the CWP, as it provides results comparable to detailed values with less than 1% difference, making it a reasonable simplification. Hisamatsu and Utsunomiya (2022) modelled CWP rigidly fixed to barge and used a drag coefficient of 0.8, as the flow was dominated by current and corresponds to a turbulent regime ($Re \approx 10^7$), making the drag mainly dependent on surface roughness. Guo et al. (2024) studied different platform configurations for OTEC system and used a drag coefficient of 1.2 and added mass of 1.0 for FRP CWP with 10 m diameter when analysed in the wave environment of the China Sea. For the current analysis, a constant drag and added mass coefficient of 1.0 were used. The mass of the two systems; spar and spar with CWP are maintained same for both the numerical models by accounting for the submerged weight of the CWP (Adiputra et al., 2024).

Table 5
Details of CWP.

	Full Scale	1:175 Scale
Weight submerged (kg)	1100	0.4752
Outer Diameter (m)	4	0.0229
Inner Diameter (m)	3.4	0.0194
Length (m)	1000	5.7143
Modulus of elasticity E (MPa)	1000	5.7143
EI (Nm^2)	6.0×10^9	3.66×10^{-2}
Cd, Ca	1.0, 1.0	

The weight of the clump is selected based on the scaled submerged weight of the pipe (Hirao et al., 2021). It may be noted that the influence of ambient flow velocity on the CWP dynamic behaviour is not accounted for in the present analysis; this aspect will be explored in future work.

2.2.2. Description of mooring

The numerical simulations were performed in two stages, each employing a different mooring configuration. In the first stage, the mooring arrangement replicated the experimental setup, where horizontal soft moorings were used to validate the numerical model against the experimental results. In the second stage, a taut mooring system was implemented to investigate the platform responses under operational and survival sea conditions. In both configurations, the moorings were modelled as linear cable elements with specified axial stiffness and initial pretension (M. Chen et al., 2026). For time domain simulations, the interaction between the floater and mooring system was computed in a coupled manner, where at each time step, the hydrodynamic forces and the restoring forces from the mooring lines were evaluated at each time step. The mooring stiffness contributions were incorporated into the system stiffness matrix, and the resulting body motions were used to update line extensions and corresponding tensions throughout the simulation. This formulation ensures a consistent coupling between the linear hydrodynamics (M. Chen et al., 2022) and the mooring restoring behavior throughout the time integration process. Hydrodynamic drag and inertia forces acting on the mooring lines were not considered in the present formulation as they are insignificant (Barrera et al., 2019) for the wave parameter considered in this study.

The soft mooring system was adopted in the experiments due to flume limitations, which restricted the use of realistic taut or slack mooring systems. Taut or semi-taut mooring systems are often preferred in deepwater applications due to reduced spatial footprint and enhanced positional stability (Hisamatsu and Utsunomiya, 2022). In one study, a 12 point (4×3) taut mooring configuration was implemented for a ship-shaped OTEC platform. Similarly, Yen and Jing (2018) investigated a semisubmersible OTEC plant with a power module that used four sets of taut mooring lines placed at 90° intervals, totalling 12 lines. The mooring system consisted of three segments: a fairlead chain, a wire rope, and an anchor chain. Station keeping and hydrodynamics being the primary purpose of the study, iterative analysis was not performed for the moorings.

In the present study, a 4×2 mooring configuration is adopted to ensure sufficient support and stability for the platform. Fig. 9 displays elevation and plan of the taut moored spar with CWP. Four fairlead positions are arranged at 90° intervals around the model at the centre of gravity of the model. Two mooring lines at each fair lead point are separated from each other by an angle of 30°. The moorings make an angle of 60° with the vertical. Static equation of equilibrium is used in selecting the initial tension (Arakkan and Chandrasekaran, 2025) and stiffness parameters of the mooring (Hisamatsu and Utsunomiya, 2022). Moorings were modelled as linear cable of stiffness 1114.75 kN/m and an initial tension of 3215 kN.

2.2.3. Random wave tests

The design wave environment for the platform requires a minimum water depth of 1000 m to achieve the necessary temperature gradient for

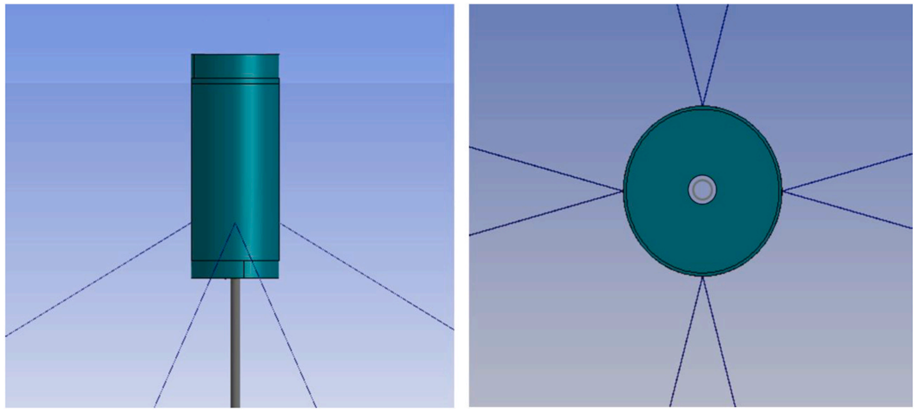

Fig. 9. Taut moored spar model with CWP.

Table 6
Details of the design wave parameters.

	Wave	Current
Operating wave condition (OC)	Hs = 5.9 m, Tp = 11.1 s JONSWAP Spectrum	2.34 m/s at SWL, 0.3 m/s near the end of cold water pipe
Survival wave parameters (SC)	Hs = 17.3 m s, Tp = 16.1 s JONSWAP Spectrum	

OTEC operation. A literature review was conducted to identify suitable design values for numerical simulation within the Indian EEZ. Vishwanath and Jalihal (2021) studied the mooring analysis of an OTEC spar desalination system, selecting a site near Chennai where India's first pilot testing of an OTEC barge was conducted. Based on their work, the operating and survival wave conditions (100-year return period) at this location were adopted for the present numerical analysis. The selected wave conditions are given in Table 6.

Table 7
Test Cases for the numerical response analysis.

Test Cases	Operational Condition		Test Cases	Survival Condition		Model
	Wave	Current		Wave	Current	
OC1	✓		SC1	✓		Spar Only
OC2	✓		SC2	✓		Spar with CWP
OC3	✓	✓	SC3	✓	✓	Spar Only
OC4	✓	✓	SC4	✓	✓	Spar with CWP

Analysis was performed first for the wave conditions without any current, to quantify the influence of CWP. Subsequently current effects were incorporated into the numerical simulation. Results are presented for both with current and without current cases for spar alone and spar with CWP. Following this, detailed numerical simulations of the taut moored spar with CWP were performed and compared with the spar only cases for operational and survival conditions. Details of the test cases considered are shown in Table 7.

Simulated random waves for operational conditions were compared with the theoretical spectrum corresponding to the input Hs and Tp parameters. The results are shown in Fig. 10, which demonstrates an

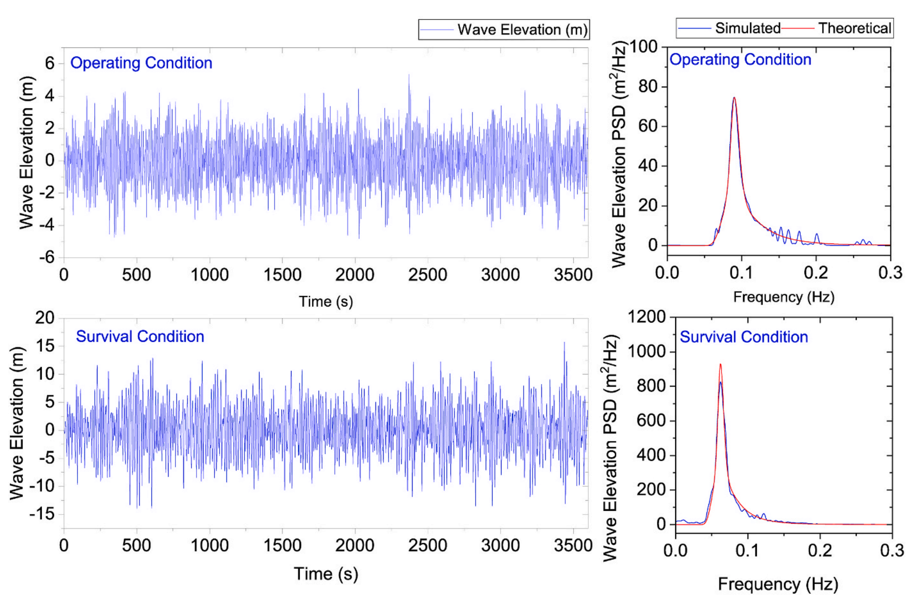

Fig. 10. Wave elevation time series and spectrum for OC and SC.

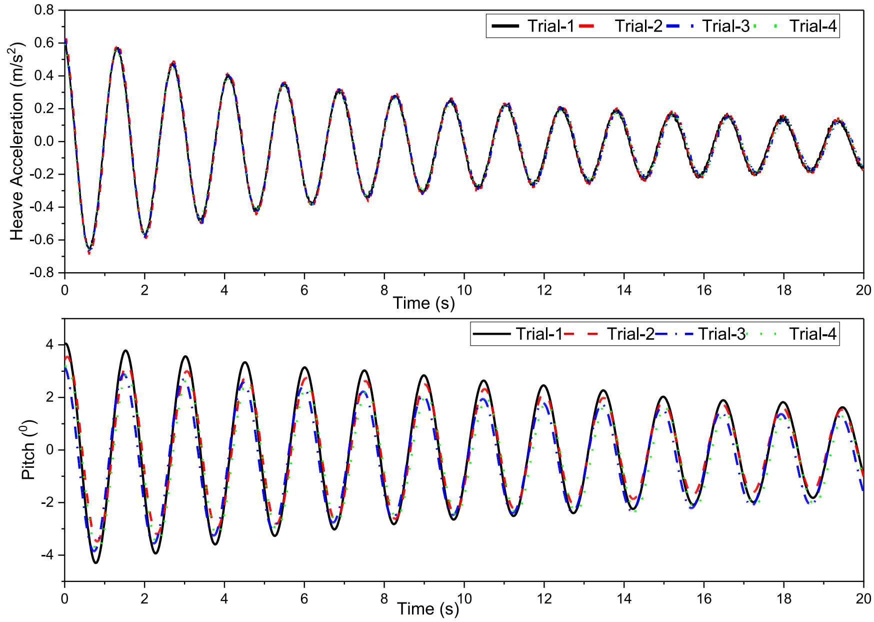

Fig. 11. Repeatability of the test results in heave and pitch decay.

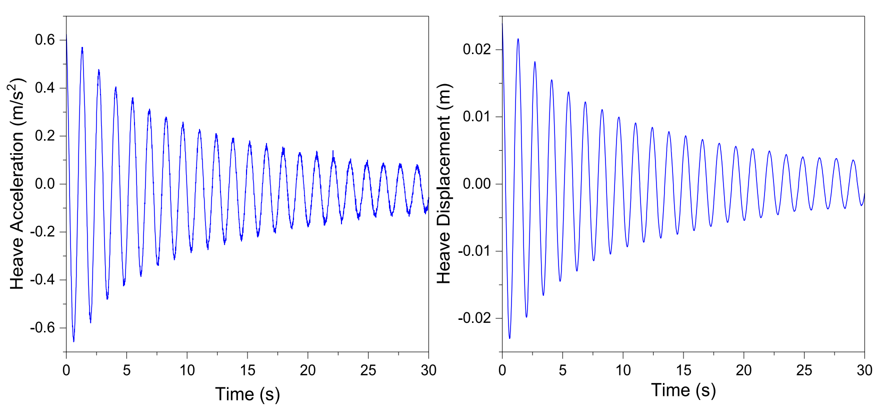

Fig. 12. Heave acceleration and corresponding displacement for a typical decay test.

acceptable agreement with the theoretical spectrum. The peak period and significant wave height (Hs) were compared, and the difference between the simulated and theoretical spectra was found to be less than 1%.

3. Results and discussions

3.1. Natural frequency and damping characteristics-experiments

This section presents the results of the experimental heave and pitch free decay tests conducted on the model (Arya et al., 2025a). Multiple trials were carried out for heave decay using known initial displacements. Specifically, four trials were conducted with initial displacements of 3 cm and 5 cm. For pitch decay, a differential motion was induced by displacing one end of the model along the x direction, and the resulting pitch angles were recorded using a motion sensor. The heave and pitch decay test results are presented in Fig. 11. The results of heave decay among various trials show excellent agreement, as identical initial displacements could be consistently applied. However, in the case of pitch, maintaining the initial angle was somewhat difficult, leading to slight variations observed in the pitch decay plot (Varley et al., 2014). Nevertheless, the natural period remained consistent across all four trials.

The accelerations recorded by the sensor were converted to corresponding displacements, and Fig. 12 shows a sample acceleration and corresponding displacement for a typical trial case.

The free decay results were used to determine the natural frequency and total damping of the system. The natural periods in heave and pitch were found to be 1.38 s and 1.46 s respectively. When scaled to the prototype, these natural periods lie outside the typical wave period range, indicating that the selected test matrix is beyond the resonance region. The damping ratio was found to be 1.72% in heave and 5.26% in pitch, suggesting comparatively higher energy dissipation in the pitch mode.

3.2. Mesh convergence

Once these preliminary decay results were obtained, numerical simulations were carried out by incorporating additional damping into the potential flow solver. A mesh sensitivity analysis was conducted, as presented in Fig. 13 (a). Four mesh sizes were evaluated, with mesh 1 representing the finest and mesh 4 the coarsest configuration. Based on the comparison, mesh 1 was selected for further analysis as it provided the best alignment with the experimental results and ensured numerical

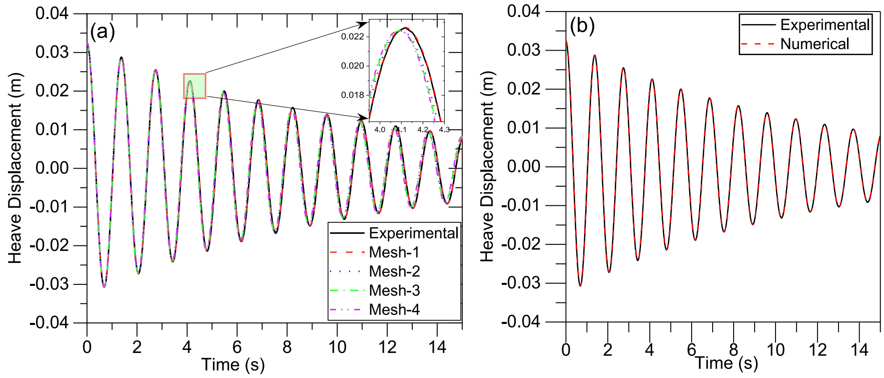

Fig. 13. (a) Mesh sensitivity analysis (b) Validation of experimental and numerical decay results.

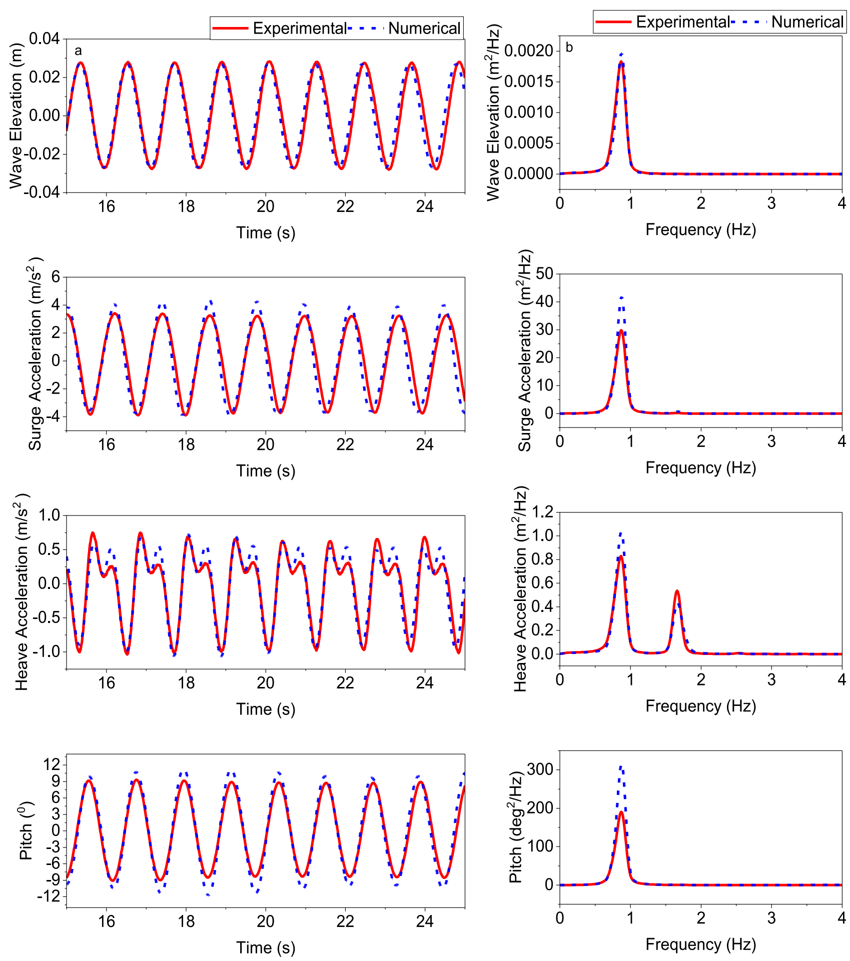

Fig. 14. Time series and PSD of measured and simulated wave elevation, surge acceleration, heave acceleration and pitch response for RW1(T = 1.18s) with wave height H = 5.14 cm.

accuracy. Fig. 13 (b) presents the comparison of simulated and experimental heave decay results, which show good agreement, thereby validating the numerical model and confirming its readiness for further simulations.

3.3. *Wave structure interaction-regular wave tests*

Fig. 14 presents the experimentally measured wave elevation, surge acceleration, heave acceleration and pitch response plotted alongside the numerically simulated results and their corresponding power spectral density (PSD) analyses. The wave elevation results show excellent agreement, while slight deviations are observed in surge, heave acceleration, and pitch displacement. These discrepancies may be attributed to the limitations of the numerical tool, particularly the assumption of frequency-independent additional viscous damping (Hegde and Nallayarasu, 2023). Second harmonics are observed in the heave acceleration similar to those reported for spar with moon pool (L. Liu et al., 2014). Such nonlinear characteristics result from the combined effect of external wave forcing and the resonance generated by the moon pool dynamics (Koo et al., 2004). As a result, the inclusion of a

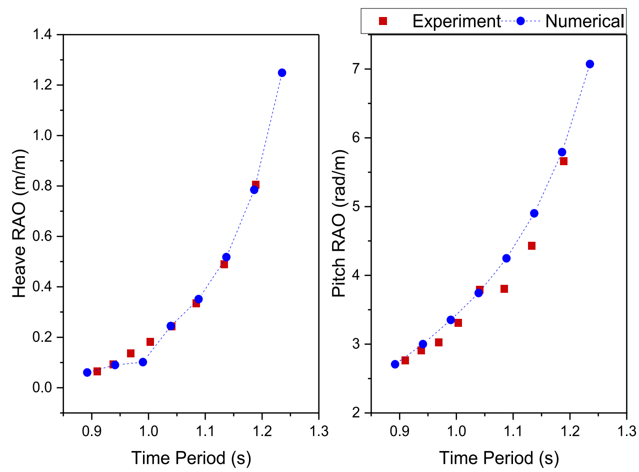

Fig. 15. Experimental and numerical RAO results of the model.

moon pool can considerably intensify or dampen the heave motion, making its influence an important factor in the design and performance evaluation of spar platforms. The peak responses in surge, heave, and pitch are observed at the wave frequency (0.847 Hz), with the occurrence of second harmonics in the measured heave accelerations indicating nonlinear behaviour (Yeung and Wang, 2018). Previous investigations have reported that spars with moon pools exhibit nonlinear heave responses at wave periods shorter than both the structural natural period and the moon pool piston mode frequency (Jiang et al., 2023; Liu et al., 2014; Liu et al., 2014, 2014) examined the heave motion of a spar across three distinct wave periods and demonstrated that nonlinear heave and moon pool water oscillations become prominent at lower periods. In agreement with these observations, the present study employs wave periods shorter than the natural heave and piston mode periods, resulting in heave motions of small amplitude and distinctly nonlinear characteristics.

3.4. Response amplitude operator (RAO)-Validation

The interaction between waves and the spar structure under regular wave conditions is most effectively described through the RAO (Hegde and Nallayarasu, 2023). To evaluate the dynamic performance, both heave and pitch RAOs were derived and compared for experimental observations and numerical predictions, as illustrated in Fig. 15. A close inspection reveals that the numerical results for pitch exhibit a slight overestimation relative to the experimental data within the wave period range of 1.05 to 1.15 s. Despite this minor deviation, the overall trend of the numerical response correlates well with the experimental time series, demonstrating consistency across both approaches. The heave RAO exhibits a better agreement between measured and simulated values, showing nearly similar response characteristics across the considered wave periods. This correlation provides validation for the adopted numerical model, allowing it to be confidently extended to perform further parametric studies and simulation scenarios, supporting its use in predicting the motion behaviour of spar platforms under varied wave conditions.

3.5. Validation of wave structure interaction with CWP

The primary focus of this paper is to understand the platform response when integrated with CWP. Since experimental limitations make physical modelling with CWP challenging, numerical simulations were performed including CWP. Hirao et al. (2021) performed both experimental and numerical simulation of a spar model with horizontal mooring. The same model is created in a potential flow based solver, and the results are compared to evaluate how effectively the existing method can simulate the behaviour. The total damping obtained from the decay experiments is used to calculate the viscous damping and given as an additional input in the solver. An additional damping of 17.55 N/m in heave and 0.08 Nms/deg in pitch direction were given. Fig. 16 shows the correlation of the present simulation with the published experimental and numerical results (Nasma et al., 2025). The peak period of the present simulations deviates slightly from the published numerical results, whereas the overall trend exhibits better agreement.

The damping parameters used in the above numerical simulation were derived from experimental results obtained at a different model scale. Specifically, the published values correspond to a 1:100 scale, while the damping parameters were determined from a 1:190 scale experiment (Nasma et al., 2025) and subsequently upscaled to match the 1:100 numerical model. This difference in scale could contribute to slight variations in damping characteristics. Furthermore, the flexibility of the CWP was not considered in the present model, which may influence the overall system stiffness and shift the peak frequency in the RAO.

3.6. Decay results-numerical simulation

The natural frequencies of the two systems; the spar with and without the CWP were determined prior to analysing the wave structure interactions (Arya et al., 2025a). Free decay tests and stability analysis

Table 8
Natural Period of the spar and spar with CWP.

Natural Period	Surge		Heave		Pitch	
	(s)	(Hz)	(s)	(Hz)	(s)	(Hz)
Spar Only	124.10	0.0081	17.99	0.0556	19.77	0.0506
Spar with CWP	133.27	0.0075	18.36	0.0545	102.81	0.0097

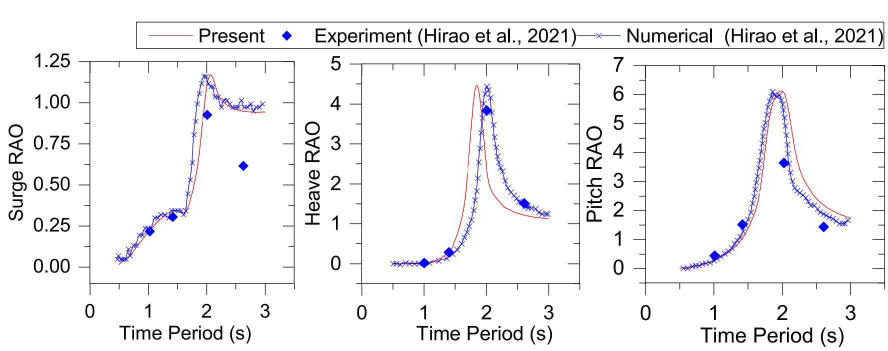

Fig. 16. RAO of spar with CWP -Re drawn based on data published (Nasma et al., 2025).

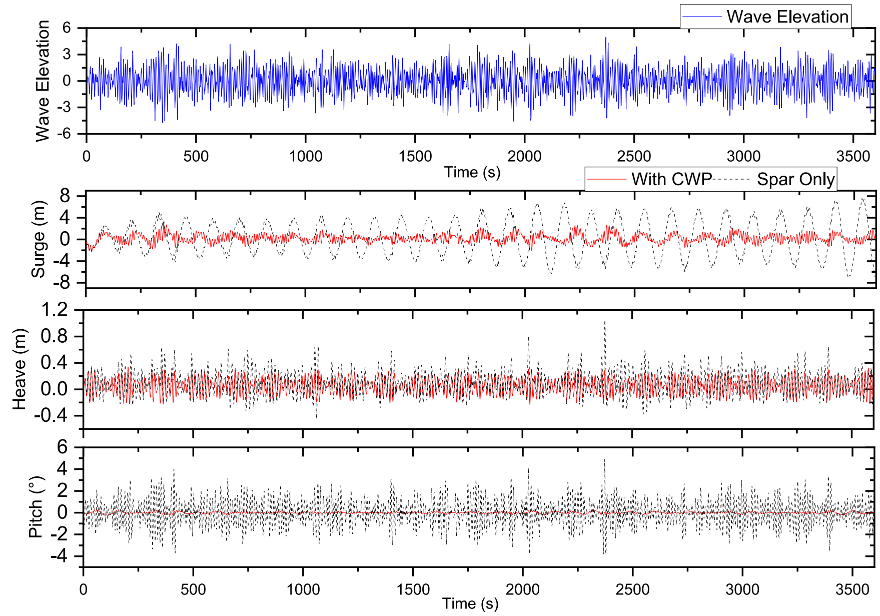

Fig. 17. Surge, heave and pitch response for operating condition (OC1 and OC2).

were performed on the numerical model. The surge, heave and pitch natural periods of the spar only case and spar with CWP are presented in. Table 8. A comparison of the two cases shows that the natural periods of heave and pitch for the spar lie within a close range and are slightly higher than the peak wave period of the selected survival condition (16.1 s). In contrast, the pitch natural period of the spar with CWP is approximately 5.5 times higher than its heave natural period. Variations in natural periods between these two configurations have been reported in previous studies (Adiputra et al., 2024) while only marginal changes in the heave period were observed in similar vessel-supported CWP systems (Hisamatsu and Utsunomiya, 2021) where the dominant motions considered were sway, heave, and roll. Significant deviations are observed in the surge and pitch periods. For both the spar and spar with CWP models, the surge natural period is substantially higher than the peak wave period and distinctly separated from the natural periods of heave and pitch.

3.7. *Motion response of taut moored spar-numerical simulation*

3.7.1. *Operational condition*

The spar model, with and without CWP, was analysed under

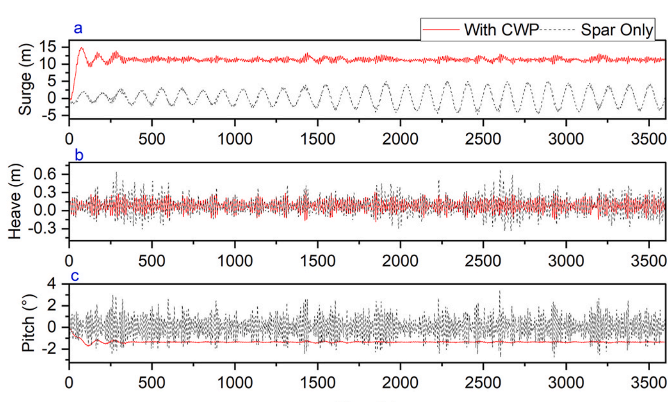

Fig. 18. Responses of Operating condition wave-current cases (OC3 and OC4): (a) surge, (b) heave and (c) pitch.

operational and survival conditions (Vishwanath and Jalihal, 2021), considering both wave-only and combined wave-current cases. The mooring parameters and configuration were kept identical for both the spar only and spar with CWP cases. The wave elevation time series for the operational conditions for wave only case is shown in Fig. 17 along with responses in surge, heave and pitch for spar only case and spar with CWP. At the outset, it is evident that all the motions response of spar with CWP differ from those of the spar only case. A significant reduction in surge and pitch motion is observed in spar with CWP. under the selected operational conditions, the mean surge and pitch responses were reduced by 84% and 95%, respectively, compared with the spar only configuration. The obtained results are aligned with the published results (Adiputra et al., 2025) on the hydrodynamics of a vessel supported OTEC system. The heave response shows marginal (27%) differences between the two model cases and remains minimal for both models, suggesting that the variations in configuration have least impact on the heave motion. The overall trend corresponds well with the published experimental results of a ship shaped floater with a CWP (Adiputra et al., 2024).

The CWP is rigidly fixed to platform and freely suspended down to deeper depth. The influence of current on the motion responses is significant, as it is a slender vertical member. Most studies on the hydrodynamics of floating OTEC and desalination systems have considered wave-current interactions (Adiputra and Utsunomiya, 2019; Hisamatsu and Utsunomiya, 2021). In the present study, the combined response under waves and a vertically varying current ranging from 2.4 m/s at the still water level to 0.3 m/s near the seabed was investigated. The surge, heave and pitch response of the cases OC3 and OC4 are shown in Fig. 18. The surge and pitch responses shifted further from their mean position compared with the spar only case. This is primarily due to the higher drag force and inertia force acting on the CWP (Faizatama et al., 2025). After omitting the initial transient portion, the mean surge and pitch responses of the spar with CWP were minimal compared to spar alone case. The heave responses exhibits largely affected by the currents with 10% higher reduction compared with wave only case. The current velocity at the still water level slightly reduced the peak response in heave for both spar only and spar with CWP cases.

Spectral analysis was performed to identify the dominant frequencies and energy distribution of the responses, thereby providing a clearer understanding of the system's dynamic behaviour under wave excitation

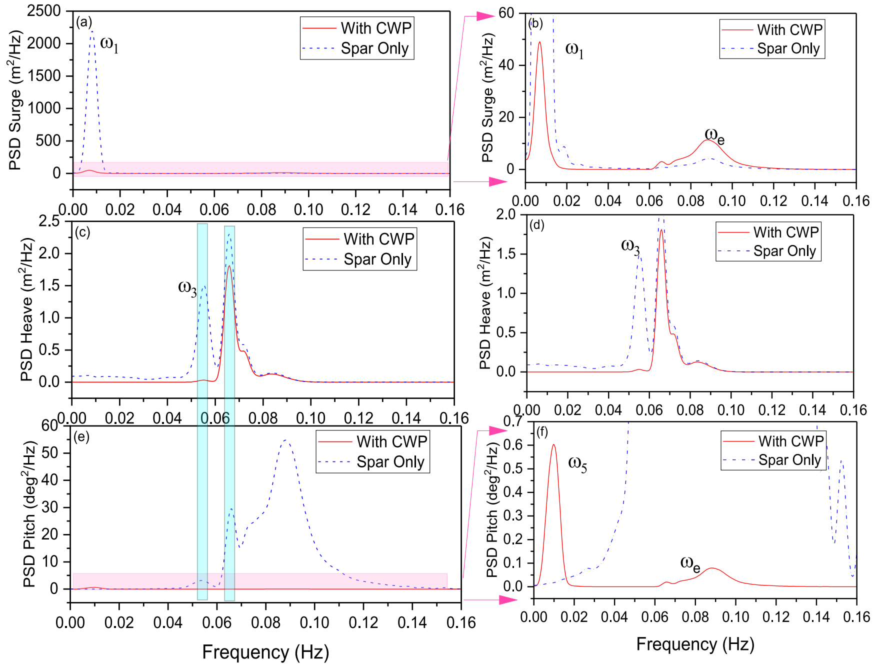

Fig. 19. Power spectral density plots of surge, heave and pitch for OC-wave case of spar with and without CWP.

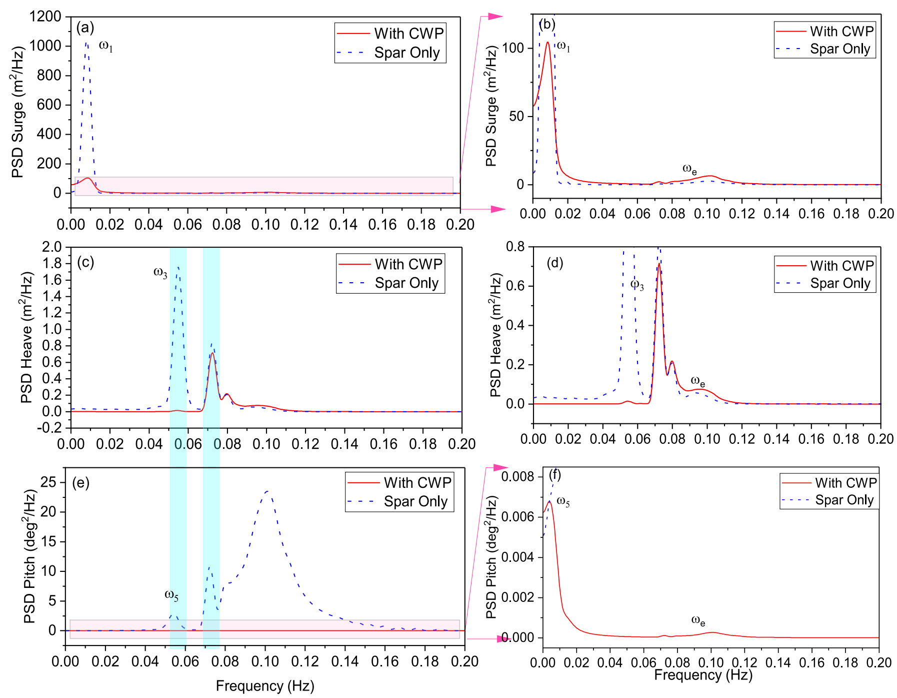

Fig. 20. Power spectral density plots of surge, heave and pitch for OC-wave-current case of spar with and without CWP (OC3 and OC4).

(Cui et al., 2025). The response spectra of the spar with and without CWP is plotted for OC-wave and OC-wave-current cases and are shown in Figs. 19 and 20 respectively.

The peak frequency of surge for spar with the CWP occurs at the surge natural frequency for both spar with and without CWP (Fig. 19(a) and (b)). The wave peak period contributes a comparatively lower amplitude in surge for spar with CWP case and is negligible for spar only case (Soeb et al., 2017). The variation of natural period of heave for spar with and without CWP is depicted in Fig. 19(c) and (d) and the coupling between heave and pitch motions can be observed from Fig. 19 (c) and (e). The pitch natural period is close to the heave natural period for the spar alone case. With the introduction of the CWP, this peak shifts away from the heave period, resulting in a decoupling of the heave and pitch motions(Fig. 19 (c) and (e)). Consequently, the responses were considerably reduced in spar with CWP cases. The peak pitch response is also distributed over a wider frequency range, on either side of the peak wave period for the spar cases. Similar trends are observed in the response results under combined wave-current interaction (Soeb et al., 2017).

In addition to the wave structure interaction, the dominant frequencies associated with the wave-current interaction of the spar only system and spar with CWP are presented in Fig. 20. When comparing the influence of wave-only and wave-current cases, the peak energy in surge and pitch is reduced under the wave-current cases for both the spar cases, while the first peak in heave appears at the heave natural period (Fig. 20 (c)). However, this trend contrasts with the pitch response of the spar. The overall response pattern, nevertheless, remains consistent with the heave and pitch motions of a spar equipped with the CWP, where a negative shift in the mean pitch response is evident from the time series data (Fig. 18). The spectral plots of surge and pitch of case OC4 is differ from those of the wave only case OC2, clearly depicting a shift in the mean response due to current action (Soeb et al., 2017) and which is minimal (Vishwanath and Jalihal, 2021) for spar only case. Under operational wave-current conditions, the heave pitch coupling in the spar (OC3) remains similar to that observed under wave-only conditions (OC1). However, this coupling is absent in the spar equipped with a CWP, leading to reduced motion amplitudes and enhanced hydrodynamic performance.

The installation of the CWP modifies the hydrodynamic behaviour of the floater by introducing additional stiffness and added mass, thereby altering the system's inertia and shifting its natural frequencies (Faizatama et al., 2025). The increased added mass tends to lower the surge and pitch natural frequencies, while changes in stiffness distribution lead to distinct variations in motion characteristics (Adiputra et al., 2024), particularly in pitch. Additionally, the CWP enhances damping through viscous drag and radiation effects (Faizatama et al., 2025), which in turn reduces the overall motion amplitudes and improves the stability of the system. This highlights the CWP's dual role as both a hydrodynamic damper and a mass-stiffness modifier in the overall system response.

3.7.2. Motion response-survival condition

Understanding the behaviour of the platform under survival condition is crucial for the stable operation of the platform for its design life period. Spar with and without CWP was subjected to waves of 17.3 m height with a peak period of 16.1 s (Vishwanath and Jalihal, 2021). The simulation results for these waves are given in Fig. 21. The response in surge, heave and pitch are significantly higher for the spar only case and is much beyond the acceptable levels of offshore platforms. With the inclusion of the CWP, the motions were considerably reduced and remained within the acceptable ranges (Vishwanath and Jalihal, 2021). The dependence of heave was found marginal in the survival condition similar to that obtained in the operational cases. With the CWP, the mean amplitude of surge, heave and pitch motions are reduced considerably. The largest percentage reduction were observed for surge and pitch which is 81% and 96% respectively. The mean amplitude of heave response in the SC2 case exhibits a 15% decrease compared with SC1. The general trend of these comparison of spar with and without CWP is consistent with the published results (Adiputra et al., 2025). This marked improvement, highlights the effectiveness of the CWP in mitigating horizontal motions and enhancing the overall stability of the platform.

Fig. 22 depicts the PSD for the two configurations (the spar and spar with CWP) in wave environment and Fig. 24 presents for wave-current survival conditions. Here, the excitation peak period is close to the peak periods of heave and pitch, resulting in a narrow energy band with very high magnitudes. Coupling between the heave and pitch motions is still observed for the spar-only cases. A close alignment between the heave and pitch frequencies outside their natural frequency range points to the presence of parametric resonance (H. Yang and Xu, 2015). This phenomenon occurs when periodic variations in system characteristics, such as stiffness or excitation forces, induce large oscillations even when the excitation frequency does not coincide with the natural frequency. In the present case, the observed behaviour appears in the vicinity of the heave natural frequency and may be associated with coupled interactions between the floating body motions and the moonpool dynamics under irregular wave excitation. (Nallayarasu & Senthil Kumar, 2017). Previous investigations have documented this effect (Davidson et al., 2022), with findings indicating that it can develop in floating platforms with circular or spar configurations (Yang and Xu, 2015). The occurrence of parametric resonance is of particular concern because it can amplify platform motions and adversely affect both stability and overall hydrodynamic performance. For the spar with CWP, surge and pitch are excited with smaller magnitudes at the peak wave period, while the heave response remains minimal. Such excitations are negligible in the spar alone cases.

Subsequently, the simulations were extended to survival wave-current cases (Fig. 23), where the surge motions became high after 2500 s for spar only cases (Soeb et al., 2017) indicating the need for

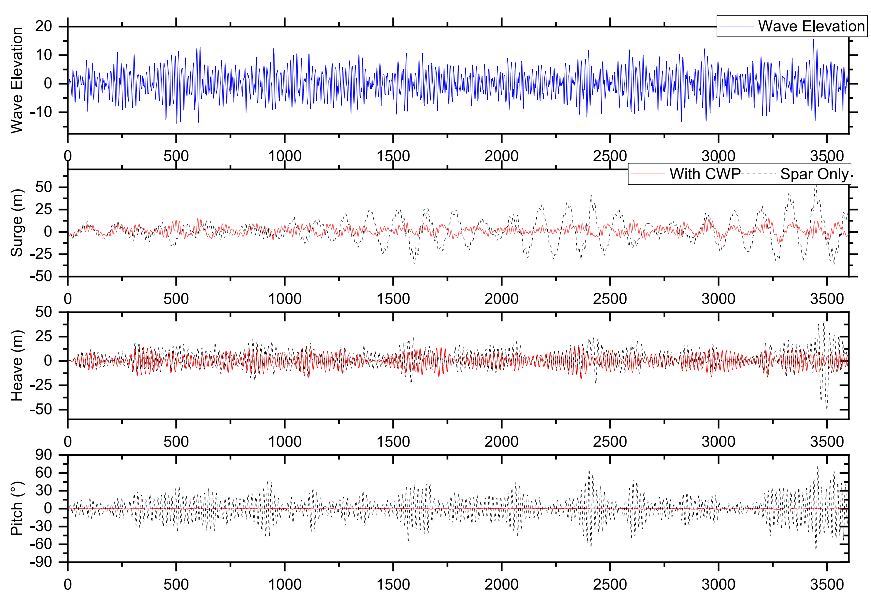

Fig. 21. Surge, pitch, heave for survival condition (SC1 and SC2).

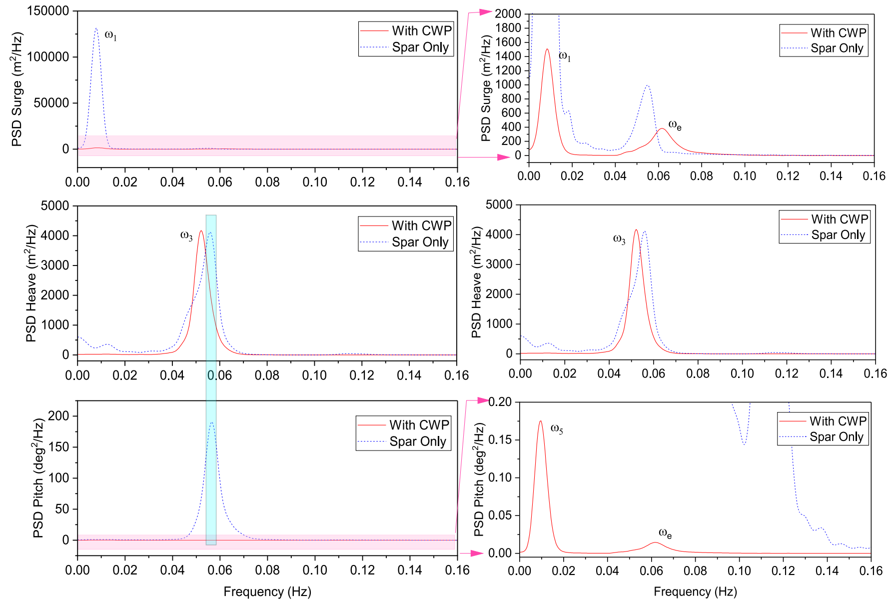

Fig. 22. Power spectral density plots of surge, heave and pitch for SC-wave case of spar with and without CWP.

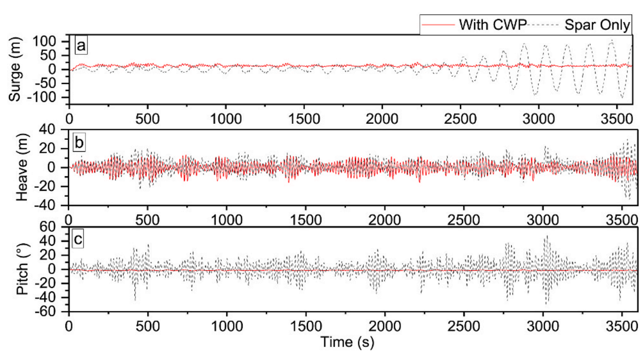

Fig. 23. Responses of Survival condition wave-current cases (SC3 and SC4):(a) surge, (b) heave and (c) pitch.

mooring system revision. The selected spar is a simple spar with moon pool with a free board of 11 m. the value of the free board should be greater than half of the maximum wave height. Under survival conditions, the mean heave amplitude of the bare spar is about 50-70% greater than its freeboard, whereas for the spar with a CWP the exceedance is comparatively lower, in the range of 30 - 40%. Consequently, the selected spar is expected to experience green water (Arya et al., 2025b; Wan et al., 2017) impact during extreme design waves. The extreme response wave spectrum illustrates the distribution of maximum responses across frequencies, highlighting the dominant excitation regions. It helps identify resonance effects, energy concentration, and the potential for critical structural loading under severe sea states. The power spectral densities are plotted for wave and wave-current conditions in the survival environment (Fig. 24). A significant reduction in mean pitch response was observed, amounting to 96% between SC1 and SC2, and 97% between SC3 and SC4. Regardless of the of simulation environment the pitch reduction between spar and spar with CWP is 95-97% across all cases.

For the cases without the CWP, the selected wave frequencies were close to the heave and pitch natural frequencies, resulting in pronounced heave-pitch coupling and amplified responses. In the present case of the spar with CWP, the shift in natural frequency eliminates the coupling effects and supresses the occurrence of parametric resonance observed in the bare spar configurations, which is an additional reason for the reduction in motion amplitudes. The installation of the CWP alters the floater's hydrodynamic characteristics by introducing additional stiffness and mass, modifying its inertia, and consequently shifting the natural frequencies. These changes, together with enhanced viscous and radiation damping (Adiputra et al., 2024; Faizatama et al., 2025) contribute to reduced motion amplitudes and improved overall stability of the system. This outcome is particularly valuable for the during the preliminary design stage, as it provides a basis for optimizing the mooring system while ensuring stability and reliable performance of the platform under varying sea states.

3.8. *Comparison of RAO of spar with and without CWP*

Accurate performance evaluation of offshore systems requires a comprehensive understanding of wave structure interactions over a broad spectrum of wave periods. To this end, simulations were performed with a regular design wave height of 5.9 m over a wide range of period from 10 to 24 s. The RAOs for all cases were determined by evaluating the ratio of the peak response amplitude to the corresponding peak wave amplitude, as obtained from the power spectral density (PSD) analysis of the simulated time series (explained in section 2.1.6). This approach ensures that the dynamic amplification of the platform response relative to the incident wave input is accurately quantified across different sea states. The following Fig. 25 presents the surge, heave and pitch RAO of the spar, spar with CWP, in wave only and wave-current environment. For the surge responses (Fig. 25 (a)), spar exhibits an undulating trend within the heave and pitch natural period range, and the coupling of surge motion with heave and pitch was observed. When the same spar was analysed with current, the predominant current velocity shifted the surge peak away from the heave and pitch natural periods. Surge RAO of spar with CWP increases gradually with increasing wave period. Comparing the surge response of spar with and without CWP, the RAO is larger at lower wave periods for spar with the CWP and smaller at higher periods. This is governed by the modified hydrodynamic characteristics of the coupled floater CWP system. In the short-period region, the free-flooded CWP changes the surge added mass, radiation damping, and excitation force balance, which may slightly amplify the response (Faizatama et al., 2025). In contrast, at longer wave periods, the increased system inertia and damping

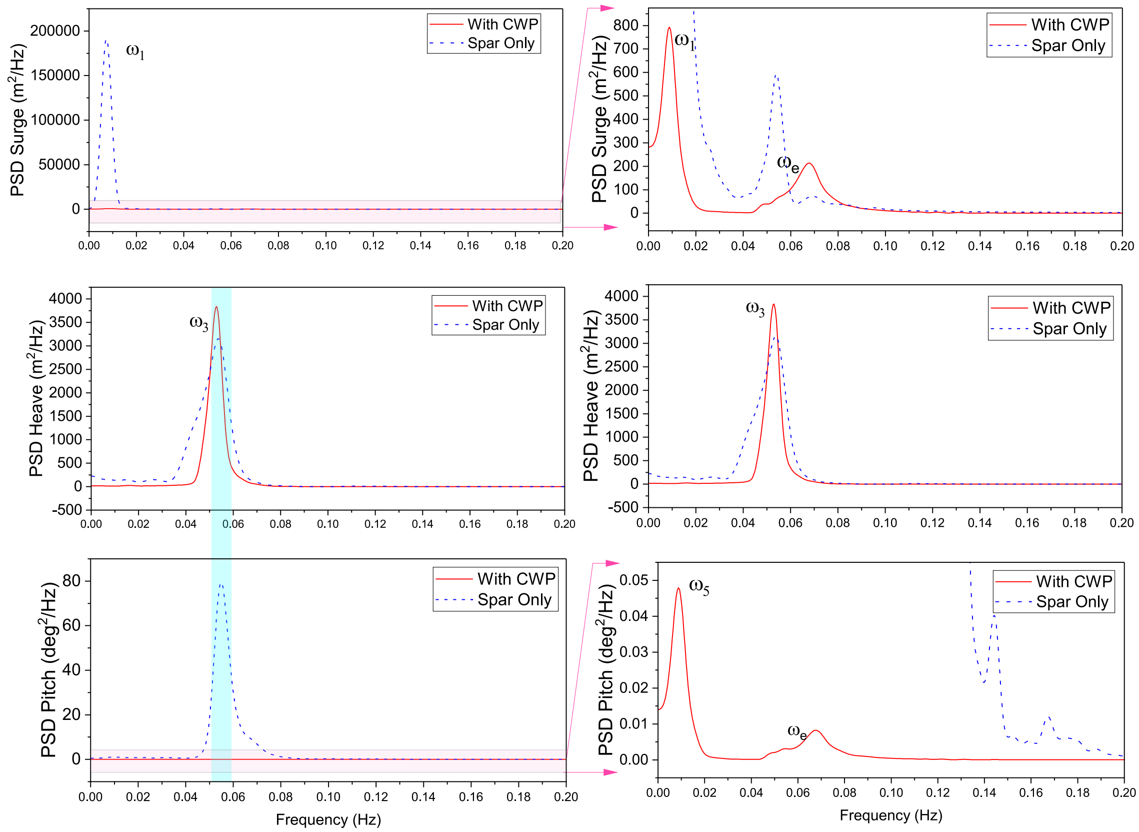

Fig. 24. Power spectral density plots of surge, heave and pitch for SC-wave-current case of spar with and without CWP.

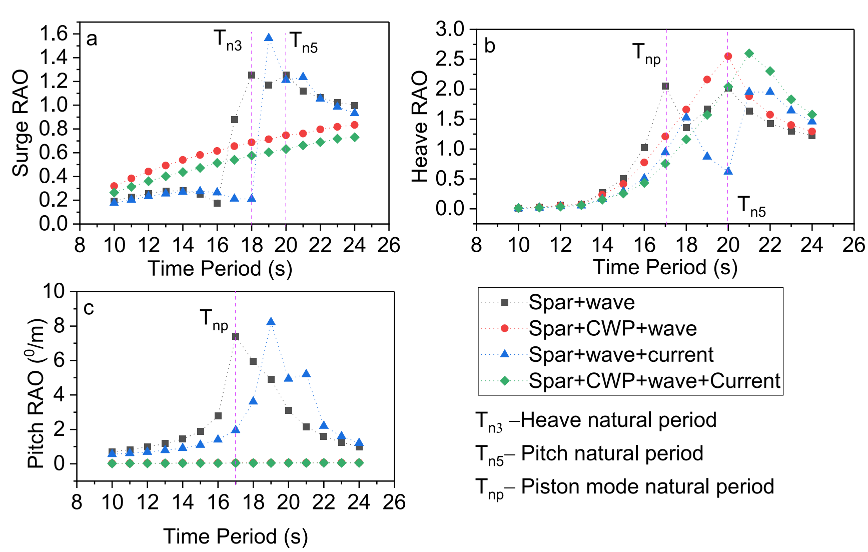

Fig. 25. RAOs of (a) surge, (b) heave and (c) pitch for the four cases.

associated with the attached CWP reduce the surge response relative to the floater without CWP. Similar trends have been observed in recent OTEC platform studies with varying CWP configurations(Faizatama et al., 2025). This underscores the need for careful dynamic analysis of the system in its intended ocean environment.

Fig. 25 (b) illustrates the heave response of the system across varying wave periods. At shorter periods (up to approximately 14 s), the influence of the CWP is minimal, whereas beyond this range, the heave response of the spar with the CWP becomes lower than that of the spar-only configuration. At higher periods, the interaction with longer waves increases the heave response (Adiputra et al., 2024). However, the heave RAO of spar with CWP shows consistent behaviour relative to the spar only case. The effect of piston mode natural frequency of the spar was evident in the heave response of spar only case, conversely this effect is absent in the spar with CWP. The coupling effects of heave and pitch periods are mitigated by the consideration CWP in the analysis. The pitch response shows a notable reduction, ranging from 20% to 50%, when the spar is configured with a CWP (Fig. 25 (c)). It is noteworthy that, for the current-included cases, the peak periods in the surge and pitch RAO plots of the spar-only configuration do not coincide with the heave or pitch natural periods. This preliminary study of the spar with the CWP highlights the significant influence and necessity of including the CWP in motion response analyses.

4. Conclusion

The study involved careful physical modelling of the OTEC spar platform, followed by detailed hydrodynamic analysis under regular wave conditions. The experimental results were validated by numerical simulations for free decay tests and wave structure interactions. Numerical simulation of the horizontally moored spar with cold water pipe (CWP) is verified against published experimental and numerical results, providing confidence to the reliability of the adopted methodology and results. A comprehensive analysis of the platform motions are carried out for spar with and without CWP considering the wave alone case and wave-current interactions. These outcome holds significant importance in the preliminary design stage, as it provides a solid basis for the optimization of the mooring system, thereby ensuring the platform's stability and consistent performance across a range of sea states. The major conclusions derived from the present study are.

- The inclusion of the CWP altered the natural periods of the spar in surge, heave, and pitch, shifting the pitch natural frequency to a lower range, well separated from heave. The spar with CWP showed no parametric resonance nor heave pitch coupling, which were evident in the bare spar case, emphasizing the importance of considering the CWP in the dynamic analysis of floating OTEC system.
- Numerical analyses of the two configurations; spar with and without the CWP under operational and survival wave conditions revealed a pronounced reduction in surge and pitch responses upon the inclusion of the CWP. The influence on heave motion remained moderate yet significant for the selected spar. Quantitatively, the inclusion of the CWP resulted in marked reductions in the mean motion amplitudes, with decreases of approximately 80-86% in surge, 15-37% in heave, and 95-97% in pitch. These findings are noteworthy, as they are directly linked to the overall performance of the system and play a crucial role in the design and optimization of the mooring arrangement.
- Under survival wave-current conditions, the spar platform exhibited very high response and instability in surge. Analysis revealed that the freeboard of the spar was lower than half of the maximum wave height in survival conditions. This indicates the strong influence of green water loading on the platform's behaviour in extreme sea states. Therefore, it is essential to design mooring systems capable of effectively mitigating such events by minimizing surge motion. A comprehensive site specific analysis should be carried out, tailored to the prevailing metocean conditions to ensure optimal performance and reliability of the platform.
- The RAO plots for different wave periods demonstrate the dependence of surge, heave, and pitch responses on the wave period. The spar with the CWP exhibited pronounced surge motion at shorter wave periods, which diminished as the wave period increased, whereas the heave response showed the opposite trend. Pitch was consistently 20-50% lesser for configuration of spar with CWP. The wave-current RAO of the spar with CWP exhibited a consistent marginal reduction in surge and pitch compared to the wave-only RAO across all periods. In contrast the heave RAO is noticed to have higher values for longer wavelengths.

The conclusion from the present numerical analysis highlights the need for understanding the OTEC platform performance by considering the CWP along with the floating body configurations. Compared to the spar with CWP, the spar-only cases tend to either overestimate or underestimate the platform responses, depending on the wave period.

4.1. Limitations and future work

The present study does not consider internal flow within the CWP or the flexibility of the pipe, both of which may influence the hydrodynamic responses more precisely. A broader parametric investigation into different CWP configurations is necessary, along with case-specific simulations to capture practical variability. The same current conditions were assumed for both operational and survival scenarios, and the influence of varying the wave and current headings remains to be examined. The present work was limited to first-order wave loading, and higher-order wave effects, including mean drift forces, difference-frequency responses, and QTF-related excitations, were not incorporated. These aspects, together with additional experimental studies including the CWP, will be examined in future investigations. Future studies should also incorporate pipe flexibility and internal flow dynamics to enhance the predictive accuracy of floating OTEC system performance.

Disclosure statement

No potential conflict of interest was reported by the author(s).

CRediT authorship contribution statement

N.V. Nasma Noor: Conceptualization, Data curation, Formal analysis, Methodology, Software, Validation, Writing – original draft, Writing – review & editing. **V.K. Srineash:** Conceptualization, Data curation, Formal analysis, Methodology, Supervision, Writing – review & editing. **Manasa Ranjan Behera:** Conceptualization, Data curation, Formal analysis, Methodology, Supervision, Writing – review & editing.

Declaration of competing interest

The authors declare that they have no known competing financial interests or personal relationships that could have appeared to influence the work reported in this paper.

Acknowledgement

The authors would like to thank and acknowledge the partial funding received from NIOT, MoES, Government of India through Grant No: NIOT/F&A/DOMV5-01. The authors would also like to express their gratitude to Ms. Deepthi Carol for her contributions to sketching the flume setup.

References

Adiputra, R., Firdaus, M.I., Firdaus, N., Prabowo, A.R., Salamena, G.G., Faizatama, A.M., 2025. Hydrodynamic responses of OTEC floating platform in operating and dismantling states. In: Kolhe, M.L. (Ed.), Proceedings of 15th International Conference on Renewable and Clean Energy (ICRCE 2025). Springer Nature, pp. 69–76. https://doi.org/10.1007/978-981-96-8154-9_8.

Adiputra, R., Imam Firdaus, M., Firdaus, N., 2024. Coupled motion analysis of a ship-shaped floater and the cold-water pipe for OTEC implementation. Ocean Space Utilizat. 4. https://doi.org/10.1115/OMAE2024-129530. V004T05A028.

Adiputra, Ristiyanto, Utsunomiya, Tomoaki, Koto, Jaswar, Yasunaga, Takeshi, Ikegami, Yasuyuki, 2019. Preliminary design of a 100 MW-net ocean thermal energy conversion (OTEC) power plant study case: Mentawai island, Indonesia. J. Mar. Sci. Technol. 25 (1), 48–68. https://doi.org/10.1007/s00773-019-00630-7. http://link.springer.com/10.1007/s00773-019-00630-7. (Accessed 19 February 2019).

Adiputra, R., Utsunomiya, T., 2019. Stability based approach to design cold-water pipe (CWP) for ocean thermal energy conversion (OTEC). Appl. Ocean Res. 92, 101921. https://doi.org/10.1016/j.apor.2019.101921.

Adiputra, R., Utsunomiya, T., 2021. Linear vs non-linear analysis on self-induced vibration of OTEC cold water pipe due to internal flow. Appl. Ocean Res. 110, 102610. https://doi.org/10.1016/j.apor.2021.102610.

Aiswaria, K., Balaji, R., Krishnendu, P., 2024. Experimental and numerical investigation of breakwater-integrated heaving point absorber device under irregular waves. Eur. J. Mech. B Fluid 107, 40–51. https://doi.org/10.1016/j.euromechflu.2024.04.014.
ANSYS, 2022. Ansys AQWA version 2022 R1.
Ansys AQWA theory manual 2022R1.
Arakkan, S., Chandrasekaran, S., 2025. Mitigating heave response for safer LNG operations: a numerical study on offshore buoyant leg storage and regasification platforms. In: *Proceedings of the Thirty-Fifth (2025) International Ocean and Polar Engineering Conference*. ISOPE 2025.
Aresti, L., Christodoulides, P., Michailides, C., Onoufriou, T., 2023. Reviewing the energy, environment, and economy prospects of ocean thermal energy conversion (OTEC) systems. Sustain. Energy Technol. Assessments 60, 103459. https://doi.org/10.1016/j.seta.2023.103459.
Arya, T., Srineash, V.K., Behera, M.R., 2025a. Effect of wind-wave interaction on the performance of SPAR type FOWT for varying mooring arrangements. Proc. IME M J. Eng. Marit. Environ., 14750902251345045 https://doi.org/10.1177/14750902251345045.
Arya, T., Srineash, V.K., Behera, M.R., 2025b. Hydrodynamics of offshore platforms: a critical review. J. Marine Eng. Technol. 0 (0), 1–19. https://doi.org/10.1080/20464177.2025.2460265.
Arya, T., Srineash, V.K., Behera, M.R., 2026. Effect of wind-wave interaction on the performance of SPAR type FOWT for varying mooring arrangements. Proc. IME M J. Eng. Marit. Environ. 240 (1), 60–78. https://doi.org/10.1177/14750902251345045.
Barr, Roderick A., Sheldon, Lewis R., 1980. Model testing of OTEC plant platform and cold water. Offshore Technol. Conf., OTC-3687-MS https://doi.org/10.4043/3687-ms, OTC. https://onepetro.org/OTCONF/proceedings/80OTC/80OTC/OTC-3687-MS/48528. (Accessed 5 May 1980).
Barrera, C., Guanche, R., Losada, I.J., 2019. Experimental modelling of mooring systems for floating marine energy concepts. Mar. Struct. 63, 153–180. https://doi.org/10.1016/j.marstruc.2018.08.003.
Bull, D., 2015. An improved understanding of the natural resonances of moonpools contained within floating rigid-bodies: theory and application to oscillating water column devices. Ocean. Eng. 108, 799–812. https://doi.org/10.1016/j.oceaneng.2015.07.007.
Cai, Q., Li, Z., Hu, J., Huang, B., Pan, Y., Wu, H., Ren, Z., 2025. Fatigue study of unbonded flexible risers for ocean thermal energy conversion based on the joint distribution of wind, wave, and current. Appl. Ocean Res. 154, 104306. https://doi.org/10.1016/j.apor.2024.104306.
Chakrabarti, S.K., 1994. (with world scientific (firm)). Offshore Structure Modeling. World Scientific Pub. Co.
Chen, M., Liu, S., Jiang, X., Hu, M., Li, Z., Jiang, J., Li, J., 2026. Comparative analysis of fully-coupled towing simulation for a 15MW floating wind turbine using FAST2AQWA method. Ocean. Eng. 347, 124003. https://doi.org/10.1016/j.oceaneng.2025.124003.
Chen, M., Xiao, P., Zhou, H., Li, C.B., Zhang, X., 2022. Fully coupled analysis of an integrated floating wind-wave power generation platform in operational sea-states. Front. Energy Res. 10, 931057. https://doi.org/10.3389/fenrg.2022.931057.
Chen, L., Basu, B., 2018. Fatigue load estimation of a spar-type floating offshore wind turbine considering wave-current interactions. Int. J. Fatig. 116, 421–428. https://doi.org/10.1016/j.ijfatigue.2018.06.002.
Choi, E.-Y., Jeong, W.-B., Cho, J.-R., 2016. Combination resonances in forced vibration of spar-type floating substructure with nonlinear coupled system in heave and pitch motion. Int. J. Nav. Archit. Ocean Eng. 8 (3), 252–261. https://doi.org/10.1016/j.ijnaoe.2016.03.004.
Chu, Y.I., Wang, C.M., 2020. Hydrodynamic response analysis of combined spar wind turbine and fish cage for offshore fish farms. Int. J. Struct. Stabil. Dynam. 20 (9), 2050104. https://doi.org/10.1142/S0219455420501047.
Chuang, T.-C., Yang, W.-H., Yang, R.-Y., 2021. Experimental and numerical study of a barge-type FOWT platform under wind and wave load. Ocean. Eng. 230, 109015. https://doi.org/10.1016/j.oceaneng.2021.109015.
Cui, Y., Li, Y., Li, G., Feng, Y., Li, H., Wang, B., Meng, H., Deng, W., 2025. Dynamic response and nonlinear resonance of cylindrical FPSO with a ring groove considering time-varying restoring stiffness. Ocean. Eng. 325, 120857. https://doi.org/10.1016/j.oceaneng.2025.120857.
Cummins, W.E., 1962. The impulse response function and ship motions. In: Symposium on Ship Theory.
Davidson, J., Kalmár-Nagy, T., Habib, G., 2022. Parametric excitation suppression in a floating cylinder via dynamic vibration absorbers: a comparative analysis. Nonlinear Dyn. 110 (2), 1081–1108. https://doi.org/10.1007/s11071-022-07710-1.
Faizatama, A.M., Firdaus, N., Adiputra, R., Prabowo, A.R., Ghanbari-Ghazijahani, T., Fazeres-Ferradosa, T., Melnyk, O., Salamena, G.G., 2025. Hydrodynamic impact of cold-water pipes and mooring systems on KVLCC2 for floating OTEC platforms. Ocean. Eng. 341, 122491. https://doi.org/10.1016/j.oceaneng.2025.122491.
Guo, H., Li, J., Liu, M., Xiao, L., Guo, L., 2024a. Experimental investigation on dynamic responses of cantilevered aspirating pipe under the combined action of internal and external flow. Ocean. Eng. 313, 119446. https://doi.org/10.1016/j.oceaneng.2024.119446.
Guo, H., Liu, M., Li, J., Guo, L., 2024b. Study on applicability of floating OTEC platform configurations. In: (2024) International Ocean and Polar Engineering Conference. Thirty-fourth.
Halkyard, John, Sheikh, Rizwan, Marinho, Thiago, Shi, Shan, Ascari, Matthew, 2014. Current developments in the validation of numerical methods for predicting the responses of an Ocean Thermal Energy Conversion (OTEC) system cold water pipe. Ocean Space Utilization; Professor Emeritus J. Randolph Paulling Honoring Symp. Ocean Technol. 7, V007T12A028. https://doi.org/10.1115/omae2014-24636, American Society of Mechanical Engineers. https://asmedigitalcollection.asme.org/OMAE/proceedings/OMAE2014/45493/San%20Francisco,%20California,%20USA/278455. (Accessed 1 October 2014).
Haripriya, R., Misra, A., Jeyaraj, S., Ramakrishnan, B., 2021. Wave energy assessment for 39 years along the exclusive economic zone (EEZ) of India. Reg. Stud. Mar. Sci. 45, 101809. https://doi.org/10.1016/j.rsma.2021.101809.
Hegde, P., Nallayarasu, S., 2023. Hydrodynamic response of buoy form spar with heave plate near the free surface validated with experiments. Ocean. Eng. 269, 113580. https://doi.org/10.1016/j.oceaneng.2022.113580.
Herrera, J., Sierra, S., Ibeas, A., 2021. Ocean thermal energy conversion and other uses of deep sea water: a review. J. Mar. Sci. Eng. 9 (4), 356. https://doi.org/10.3390/jmse9040356.
Hirao, S.C., Umeda, J., Kokubun, K., Fujiwara, T., 2021. Tank test and numerical simulation of spar type floating OTEC. Ocean Renew. Energy 9. https://doi.org/10.1115/OMAE2021-62107. V009T09A004.
Hisamatsu, R., Utsunomiya, T., 2021. Simplified formulation of coupled system between moored ship and elastic pipe for OTEC plantship. Ocean Space Utilizat. ume 5. https://doi.org/10.1115/OMAE2021-62122. V005T05A011.
Hisamatsu, R., Utsunomiya, T., 2022. Coupled response characteristics of cold water pipe and moored ship for floating OTEC plant. Appl. Ocean Res. 123, 103151. https://doi.org/10.1016/j.apor.2022.103151.
Hong, S., Kim, J.H., Hong, S.W., Jalihal, P., Ravindran, M., 2004, May 23. A hybrid model test of a deep water OTEC mooring system. In: The Fourteenth International Offshore and Polar Engineering Conference. Toulon, France, May 2004.
ITTC, 2017. Recommended Procedures and guidelines-floating Offshore Platform Experiments.
Jiang, S.-C., Ran, Y.-Q., Feng, A., 2023. On the hydrodynamic behaviour of second-order harmonic induced sloshing-mode resonance in moonpool. Mar. Struct. 92, 103503. https://doi.org/10.1016/j.marstruc.2023.103503.
Jung, D., Park, H., Koterayama, W., Kim, H., 2005. Vibration of highly flexible free hanging pipe in calm water. Ocean. Eng. 32 (14–15), 1726–1739. https://doi.org/10.1016/j.oceaneng.2005.02.005.
Kaptan, M., Skaare, B., Jiang, Z., Ong, M.C., 2022. Analysis of spar and semi-submersible floating wind concepts with respect to human exposure to motion during maintenance operations. Mar. Struct. 83, 103145. https://doi.org/10.1016/j.marstruc.2021.103145.
Koo, B.J., Kim, M.H., Randall, R.E., 2004. The effect of nonlinear multi-contact coupling with gap between risers and guide frames on global spar motion analysis. Ocean. Eng. 31 (11–12), 1469–1502. https://doi.org/10.1016/j.oceaneng.2004.01.002.
Lee, D.Y., Nam, B.W., Jung, D.H., Hong, S.Y., Kim, H., 2015. An experimental study on the motion response of OTEC platforms. In: Proceedings of the twenty-fifth (2015) International Ocean and Polar Engineering Conference Kona, Big Island, Hawaii, USA. June 21-26, 2015.
Lee, S.-H., Hwang, S., Kim, H.-S., Hyun, Y.-J., Lee, S.-K., Paik, K.-J., 2023. A numerical study on the hydrodynamic performance of a tanker in bow sea conditions depending on restraint conditions. J. Mar. Sci. Eng. 11 (9), 1726. https://doi.org/10.3390/jmse11091726.
Li, C.B., Choung, J., 2021. Effects of strain- and strain rate- dependent nonlinear mooring line stiffness on floating platform motion. Ocean. Eng. 241, 110011. https://doi.org/10.1016/j.oceaneng.2021.110011.
Liang, N.K., Peng, H.K., 2023. A preliminary study on floating flexible OTEC cold water pipe. J. Mar. Sci. Technol. 31 (4). https://doi.org/10.51400/2709-6998.2710.
Liu, H., Chen, M., Han, Z., Zhou, H., Li, L., 2022. Feasibility study of a novel open ocean aquaculture ship integrating with a wind turbine and an internal turret mooring system. J. Mar. Sci. Eng. 10 (11), 1729. https://doi.org/10.3390/jmse10111729.
Liu, L., Incecik, A., Zhang, Y., Tang, Y., 2014. Analysis of heave motions of a truss spar platform with semi-closed moon pool. Ocean. Eng. 92, 162–174. https://doi.org/10.1016/j.oceaneng.2014.09.048.
Liu, W., Ding, J., Fu, J., Zhang, Z., Yu, J., Hu, H., Bashir, M., Li, S., Yang, Y., 2025. Comparison of the fully coupled dynamic responses of spar-type integrated wind-current floating energy systems with various tidal turbine layouts. Ocean. Eng. 325, 120866. https://doi.org/10.1016/j.oceaneng.2025.120866.
Ma, Y., You, Y., Zhang, J., Chen, K., Feng, A., 2023. Experimental study on dynamic stability of vertical cantilevered pipe aspirating fluid immersed in various water depths. Ocean. Eng. 272, 113378. https://doi.org/10.1016/j.oceaneng.2022.113378.
Ma, Q.W., Patel, M.H., 2001. On the non-linear forces acting on a ¯oating spar platform in ocean waves. Appl. Ocean Res. 23.
Manolache, A.I., Andrei, G., 2024. A comprehensive review of multi-use platforms for renewable energy and aquaculture integration. Energies 17 (19), 4816. https://doi.org/10.3390/en17194816.
Maris, A.T., Paulling, J.R., 1980. Analysis and design of the cold-water pipe (CWP) for the OTEC system with application to OTEC-1. Marine Technol. SNAME News 17 (3), 281–289. https://doi.org/10.5957/mt1.1980.17.3.281.
Miller, A., Ascari, M., 2011. OTEC advanced composite cold water pipe: final technical report (Final Technical Report, 1024183; p. Final Technical Report, 1024183). https://doi.org/10.2172/1024183.
Nallayarasu, S., Kumar, N.S., 2017. Experimental and numerical investigation on hydrodynamic response of buoy form spar under regular waves. Ships Offshore Struct. 12 (1), 19–31. https://doi.org/10.1080/17445302.2015.1099227.
Nallayarasu, S., Senthil Kumar, N., 2017. Experimental and numerical investigation on hydrodynamic response of buoy form spar under random waves. Ships Offshore Struct. 12 (5), 734–746. https://doi.org/10.1080/17445302.2016.1218600.
Nasma, N.N., Srineash, V., Behera, M.R., 2025. Hydrodynamic performance analysis of floating platform for OTEC application. In: Thirty-Fifth (2025) International Ocean

and Polar Engineering Conference. ISOPE. In: https://onepetro.org/ISOPEIOPEC/proceedings/ISOPE25/ISOPE25/ISOPE-I-25-099/713297.

Nasma Noor, N.V., Srineash, V.K., Behera, M.R., 2024. Hydrodynamics of floating offshore OTEC platforms – a review. Ships Offshore Struct. 1–17. https://doi.org/10.1080/17445302.2024.2398131.

Nihous, G.C., Vega, L.A., 1993. Design of a 100 MW OTEC-Hydrogen plantship. Mar. Struct. 6 (2–3), 207–221. https://doi.org/10.1016/0951-8339(93)90020-4.

O'Donnell, D., Murphy, J., Pakrashi, V., 2021. Comparison of response amplitude operator curve generation methods for scaled floating renewable energy platforms in ocean wave basin. ASME Lett. Dyn. Syst. Control 1 (2), 021012. https://doi.org/10.1115/1.4049169.

Pesce, C.P., Martins, C.A., 2005. Numerical computation of riser dynamics. In: Chakrabarti, S.K. (Ed.), WIT Transactions on State of the Art in Science and Engineering, first ed., vol. 1. WIT Press, pp. 253–309. https://doi.org/10.2495/978-1-85312-837-0/07.

Pham, T.D., Shin, H., 2019. A new conceptual design and dynamic analysis of a spar-type offshore wind turbine combined with a moonpool. Energies 12 (19), 3737. https://doi.org/10.3390/en12193737.

Rambabu, N., Srineash, V.K., 2025. Numerical investigation on the hydrodynamics of vertical seawalls defended by a submerged breakwater. J. Waterw. Port, Coast. Ocean Eng. 151 (1), 04024020. https://doi.org/10.1061/JWPED5.WWENG-2144.

Rony, J.S., Arya, T., Sashank, R., Srineash, V.K., Behera, M.R., 2026. Experimental investigation of dynamic characteristics of OC-3 spar platform subjected to aero-hydrodynamic loading. J. Offshore Mech. Arctic Eng. 1–47. https://doi.org/10.1115/1.4071880.

Salama, Mamdouh M., Stjern, Gisle, Storhaug, Turid, Spencer, Brian, Echtermeyer, Andreas, 2002. The first offshore field installation for a composite riser joint. In: Offshore Technology Conference, OTC 14018, vol. 1, p. 234.

Sashank, R., Rony, J.S., Rambabu, N., Srineash, V.K., 2026. Hydrodynamic performance of an oscillating water column with power take-off interaction: an experimental investigation. Renew. Energy 256, 124095. https://doi.org/10.1016/j.renene.2025.124095.

Shahabadi, M., shadlaghani, A., Mansoorzadeh, S., 2017. Evaluation of moonpool effects on hydrodynamic resistance of a supply vessel, using experimental and numerical methods. Int. J. Marit. Technol. 7, 1–9. https://doi.org/10.18869/acadpub.ijmt.7.1.

Shi, S., Halkyard, J., Kurup, N., Jiang, L., 2012. Coupled analysis approach in OTEC system design. In: Ronald, W. (Ed.), Yeung Honoring Symposium on Offshore and Ship Hydrodynamics, vol. 4. Offshore Geotechnics, pp. 795–802. https://doi.org/10.1115/OMAE2012-83978.

Soeb, M.R., Islam, A.B.M.S., Jumaat, M.Z., Huda, N., Arzu, F., 2017. Response of nonlinear offshore spar platform under wave and current. Ocean. Eng. 144, 296–304. https://doi.org/10.1016/j.oceaneng.2017.07.042.

Spanos, Pol D., Nava, Vincenzo, Arena, Felice, 2010. Coupled surge-heave-pitch dynamic modeling of spar-moonpool-riser interaction. J. Offshore Mech. Arctic Eng. 133 (2), 021301. https://doi.org/10.1115/1.4001956. https://asmedigitalcollection.asme.org/offshoremechanics/article/doi/10.1115/1.4001956/435668/Coupled-SurgeHeavePitch-Dynamic-Modeling-of. (Accessed 6 December 2010).

Sreelakshmi, S., Bhaskaran, P.K., 2020. Regional wise characteristic study of significant wave height for the Indian Ocean. Clim. Dyn. 54 (7–8), 3405–3423. https://doi.org/10.1007/s00382-020-05186-6.

Tarnopol'skii, Yu M., Kulakov, V.L., Mungalov, D.D., 1999. Composites in offshore technology in the next century. Mech. Compos. Mater. 35 (5), 365–372. https://doi.org/10.1007/BF02329321.

Thomas, A., Srineash, V.K., Behera, M.R., 2024. Numerical investigation on hydrodynamic response of a SPAR platform for offshore wind energy. Ocean Syst. Eng. 14 (3), 211–235. https://doi.org/10.12989/OSE.2024.14.3.211.

Varley, R., Halkyard, J., Johnson, P., Shi, S., Marinho, T., 2014. John Halkyard and Associates, Houston, TX (United States), BMT Scientific Marine Services, Inc., Houston, TX (United States), Houston Offshore Engineering, Houston, TX (United States), & Federal Univ. of Rio de Janeiro (Brazil). LabOceano. In: OTEC Cold Water Pipe-Platform Subsystem Dynamic Interaction Validation (DE–EE0003637, 1326856; P. DE–EE0003637, 1326856). https://doi.org/10.2172/1326856.

Vishwanath, A., Jalihal, P., 2021. Nonlinear analysis of mooring system for an offshore desalination platform. In: Saha, S.K., Mukherjee, M. (Eds.), Recent Advances in Computational Mechanics and Simulations. Springer, Singapore, pp. 95–106.

Vishwanath, A., Jalihal, P., 2022. Studies on platform configurations for offshore energy and desalination applications. OCEANS 2022 - Chennai 1–8. https://doi.org/10.1109/OCEANSChennai45887.2022.9775248.

Wan, L., Greco, M., Lugni, C., Gao, Z., Moan, T., 2017. A combined wind and wave energy-converter concept in survival mode: numerical and experimental study in regular waves with a focus on water entry and exit. Appl. Ocean Res. 63, 200–216. https://doi.org/10.1016/j.apor.2017.01.013.

Wang, G., Bar, D., Schreier, S., 2024. The potential of end-of-life ships as a floating seawall and the methodical use of gap resonance for wave attenuation. Ocean. Eng. 298, 117246. https://doi.org/10.1016/j.oceaneng.2024.117246.

Wang, J., Xiang, S., Fu, S., Cao, P., Yang, J., He, J., 2016. Experimental investigation on the dynamic responses of a free-hanging water intake riser under vessel motion. Mar. Struct. 50, 1–19. https://doi.org/10.1016/j.marstruc.2016.06.003.

Ward, E.G., Ochoa, O.A., Kim, W., Gilbert, R.M., Jain, A., Miller, C., Denison, E., 2007. A Comparative Risk Analysis of Composite and Steel Production Risers. Texas A&M University, College Station, TX, USA.

Wu, S., 2020. Design considerations for the configuration of a production riser for deepsea mining of polymetallic nodules. *Day 2 Tue, May 05, 2020*, D021S025R007. https://doi.org/10.4043/30625-MS.

Xiang, Sherry, Cao, Peimin, Erwin, Richard, Kibbee, Steve, 2013. OTEC cold water pipe global dynamic design for ship-shaped vessels. Ocean Renew. Energy 8, V008T09A060. https://doi.org/10.1115/omae2013-10927, American Society of Mechanical Engineers. https://asmedigitalcollection.asme.org/OMAE/proceedings/OMAE2013/55423/Nantes,%20France/271693. (Accessed 26 November 2013).

Xu, X., Day, S., 2021. Experimental investigation on dynamic responses of a spar-type offshore floating wind turbine and its mooring system behaviour. Ocean. Eng. 236, 109488. https://doi.org/10.1016/j.oceaneng.2021.109488.

Yang, M., Teng, B., Ning, D., Shi, Z., 2012. Coupled dynamic analysis for wave interaction with a truss spar and its mooring line/riser system in time domain. Ocean. Eng. 39, 72–87. https://doi.org/10.1016/j.oceaneng.2011.11.002.

Yang, H., Xu, P., 2015. Effect of hull geometry on parametric resonances of spar in irregular waves. Ocean. Eng. 99, 14–22. https://doi.org/10.1016/j.oceaneng.2015.03.006.

Yeh, R.-H., Su, T.-Z., Yang, M.-S., 2005. Maximum output of an OTEC power plant. Ocean. Eng. 32 (5–6), 685–700. https://doi.org/10.1016/j.oceaneng.2004.08.011.

Yen, K., Jing, X., 2018. The feasibility study of OTEC integration on a semi-submersible O&G production platform. Offshore Technol. Conf. Asia, D011S004R003. https://doi.org/10.4043/28434-ms, OTC. https://onepetro.org/OTCASIA/proceedings/18OTCA/18OTCA/D011S004R003/179533. (Accessed 20 March 2018).

Yeung, R.W., Wang, L., 2018. Radiation and exciting forces of axisymmetric structures with a moonpool in waves: keynote contribution for the international workshop on wave loads and motions of ships and offshore structures, harbin, China, 5-7 November, 2017. J. Mar. Sci. Appl. 17 (3), 297–311. https://doi.org/10.1007/s11804-018-0043-3.

Yin, D., Passano, E., Lie, H., Grytøyr, G., Aronsen, K., Tognarelli, M., Kebadze, E.B., 2019. Experimental and numerical study of a top tensioned riser subjected to vessel motion. Ocean. Eng. 171, 565–574. https://doi.org/10.1016/j.oceaneng.2018.12.029.

Yue, M., Liu, Q., Li, C., Ding, Q., Cheng, S., Zhu, H., 2020. Effects of heave plate on dynamic response of floating wind turbine spar platform under the coupling effect of wind and wave. Ocean. Eng. 201, 107103. https://doi.org/10.1016/j.oceaneng.2020.107103.

Zeng, X., Shao, Y., Feng, X., Xu, K., Jin, R., Li, H., 2024. Nonlinear hydrodynamics of floating offshore wind turbines: a review. Renew. Sustain. Energy Rev. 191, 114092. https://doi.org/10.1016/j.rser.2023.114092.

Zhai, H., Yan, C., Shi, W., Zhang, L., Zeng, X., Han, X., Michailides, C., 2025. Experimental study on the hydrodynamic analysis of a floating offshore wind turbine under focused wave conditions. Energies 18 (15), 4140. https://doi.org/10.3390/en18154140.

Zhang, Y., Zheng, M., Zhang, L., Zhang, C., Tan, J., Zhang, Y., Duan, M., 2023. Investigation of dynamic behavior of ultra-large cold-water pipes for ocean thermal energy conversion. Dynamics 3 (3), 468–488. https://doi.org/10.3390/dynamics3030025.